



**A new ice-rafted
debris provenance
proxy**

A. Müller and J. Knies

Trace elements and cathodoluminescence of detrital quartz in Arctic marine sediments – a new ice-rafted debris provenance proxy

A. Müller^{1,2} and J. Knies¹

¹Geological Survey of Norway, Postboks 6315 Sluppen, 7491 Trondheim, Norway

²Natural History Museum of London, London SW7 5BD, UK

Received: 3 July 2013 – Accepted: 3 July 2013 – Published: 24 July 2013

Correspondence to: A. Müller (axel.muller@ngu.no)

Published by Copernicus Publications on behalf of the European Geosciences Union.

Title Page

Abstract

Introduction

Conclusions

References

Tables

Figures



Back

Close

Full Screen / Esc

Printer-friendly Version

Interactive Discussion



Abstract

The records of ice-rafted debris (IRD) provenance in the North Atlantic – Barents Sea allow the reconstruction of the spatial and temporal changes of ice-flow drainage patterns during glacial and deglacial periods. In this study a new approach to characterisation of the provenance of detrital quartz grains in the fraction > 500 µm of marine sediments offshore of Spitsbergen is introduced, utilizing scanning electron microscope backscattered electron and cathodoluminescence (CL) imaging, combined with laser ablation inductively-coupled plasma mass spectrometry. Based on their micro-inclusions, CL and trace element characteristics the investigated IRD grains can be classified into five distinct populations. Three of the populations are indicative of potential IRD provenance provinces in the Storfjord area including Barentsøya and Egdeøya. The results imply that under modern (interglacial) conditions IRD deposition along the western Spitsbergen margin is mainly governed by the East Svalbard Current controlling the ice-drift pattern. The presence of detrital quartz from local provinces, however, indicates that variations in IRD supply from western Spitsbergen may be quantified as well. In this pilot study it is demonstrated that this new approach applied on Arctic continental margin sediments, bears a considerable potential for the definition of the sources of IRD and thus of spatial/temporal changes in ice-flow drainage patterns during glacial/interglacial cycles.

1 Introduction

Provenance studies of ice-rafted debris (IRD) in the North Atlantic – Barents Sea are a remarkable tool for providing insights into the dynamics of large ice-sheets and the timing and duration of their disintegration (e.g. Hemming, 2004 for a review). Prominent IRD layers in the North Atlantic – the sedimentological expression of ice-sheet surging during a Heinrich event – and their origins illustrate the complexity of ice-sheet–ocean interactions in the Northern Hemisphere during the last glacial period

A new ice-rafted debris provenance proxy

A. Müller and J. Knies

Title Page

Abstract

Introduction

Conclusions

References

Tables

Figures



Back

Close

Full Screen / Esc

Printer-friendly Version

Interactive Discussion



(e.g. Andrews et al., 2009; Grousset et al., 1993; Lang Farmer et al., 2003; Peck et al., 2007; Verplanck et al., 2009).

Identifying the provenance of such IRD layers in the Arctic is, however, not straightforward because of the abundance of IRD from both sea ice and glacial rafting. The utility of isotope-based (Sr, Nd) provenance determination (Tütken et al., 2002), bulk/clay mineralogy (Nørgaard-Pedersen et al., 1998; Vogt et al., 2001) and iron grain chemical fingerprinting (Darby et al., 2002) have demonstrated their potential to provide insights into both ice drift and ice-sheet history in the circum-Arctic. However, detrital quartz grains of the > 500 µm IRD fraction, derived from icebergs and/or sea ice (Elverhøi et al., 1995; Hebbeln et al., 1998) have not been studied so far for determining sediment provenance.

Quartz is a mineral preferred for provenance studies due to its resistance to weathering and common presence in rocks and soils. The structural analysis of detrital quartz grains in sedimentary rocks by means of optical microscopy, scanning electron microscopy (SEM) and cathodoluminescence (CL) has a long history in provenance evaluation in sedimentology (e.g. Seyedolali et al., 1997; Götze and Zimmerle, 2000 and references therein). Recent developments of micro beam techniques, such as laser ablation inductively-coupled plasma mass spectrometry (LA-ICP-MS) and secondary ion mass spectrometry enable the chemical characterisation of quartz grains down to ~ 100 µm in size. Chemical analyses have shown that the trace element signature of quartz is controlled by the physicochemical conditions of quartz formation (e.g. Götze, 2009 and references therein) and, thus, represents a geochemical fingerprint of the quartz origin. However, the chemical characterisation of quartz grains by these analytical techniques has not been applied for provenance studies so far.

Here, we focus on detrital quartz grains in the > 500 µm fraction of marine sediments offshore of Spitsbergen considered to be IRD derived from melting icebergs and sea ice (cf. Elverhøi et al., 1995). Potential source rocks are constrained by introducing a new analytical approach combining structural studies of quartz grains by optical microscopy, scanning electron microscope backscattered electron imaging (SEM-BSE),

CPD

9, 4145–4189, 2013

A new ice-rafted debris provenance proxy

A. Müller and J. Knies

Title Page

Abstract

Introduction

Conclusions

References

Tables

Figures



Back

Close

Full Screen / Esc

Printer-friendly Version

Interactive Discussion



scanning electron microscope cathodoluminescence imaging (SEM-CL) with chemical analyses of quartz grains by laser ablation inductively-coupled plasma mass spectrometry (LA-ICP-MS). Up to now, we have studied 9 core-top (0–1 cm) samples randomly distributed along the western and southern coast of Spitsbergen (Fig. 1) and compared the quartz properties in the > 500 µm fraction with 18 onshore samples from potential source areas in central, west, south and southeast Spitsbergen. Our results show that various bedrock provinces in the study area are identifiable in the quartz grains offshore of Spitsbergen. Long-distance transport by sea ice is the dominant transport mechanism for the quartz grains. In addition, quartz grains released from melting icebergs/sea ice, originating from either central or southeastern Spitsbergen, are clearly recognized. Considering the complicated glacial dynamics of former Barents Sea ice sheets as recently outlined by Dowdeswell et al. (2010), this new approach applied to Arctic continental margin sediments will help to define the sources of IRD and thus spatial/temporal changes in ice-flow drainage patterns.

2 Physiogeographic setting

2.1 Geology

Spitsbergen, the main Island of the Svalbard Archipelago east of the Fram Strait forms the northwestern edge of the Barents Sea (Fig. 1a). Its geological range provides an almost complete succession from Precambrian to Quaternary strata (Steel and Worsley, 1984; Dallmann, 1999). Precambrian metamorphic crystalline rocks of the Heckla–Hoek group and sand-siltstones of Devonian ages prevail in the northern and northwestern part. Nearly undisturbed strata of Mesozoic sedimentary rocks dominate the central and southern parts of the island, while tertiary organic-rich siliciclastic rocks with coal seams dominate the inner part of southern Spitsbergen (Michelsen and Kho-rasani, 1991). The sea floor in the northwestern Barents Sea consists of Pleistocene moraines and of Holocene deposits including reworked morainic material (Dibner et al.,

CPD

9, 4145–4189, 2013

A new ice-rafted debris provenance proxy

A. Müller and J. Knies

Title Page

Abstract

Introduction

Conclusions

References

Tables

Figures



Back

Close

Full Screen / Esc

Printer-friendly Version

Interactive Discussion



1970; Bjørlykke and Elverhøi, 1975). Geophysical data indicate the presence of Mesozoic sediments immediately below the Pleistocene cover (Sundvor, 1974).

2.2 Oceanography

The North Atlantic drift carries warm and saline Atlantic water northwards. One of its main branches i.e. the West Spitsbergen Current (WSC) (Fig. 1b), is defined by having temperatures $> 2^{\circ}\text{C}$ and salinities > 34.9 psu (Schlichtholz and Goszczko, 2006). Separated by the polar front, colder ($T < 0^{\circ}\text{C}$ and salinity < 34.4 psu) and ice covered Arctic waters cross the northern Barents Sea and joins the East Spitsbergen Current (ESC) (Fig. 1b). The ESC flows southward along the SE coast of Spitsbergen and transports cold water from the Arctic Ocean, which mixes with ambient water including fresh water outflow from fjords as it continues northward along the continental shelf off Spitsbergen (Skogseth, 2003). The density barrier separates the warm, saline Atlantic water from the relatively cold, fresh Arctic water on the shelf. The frontal region prevents intrusions of warm Atlantic water into the shelf and fjord region during winter. During winter (January–March) the ice edge in the Barents Sea achieves its maximum southward extent. This zone, where the ice edge is most frequently located during spring is referred to as the marginal ice zone. Because the marginal ice zone is topographically trapped, its location during maximum extent is fairly constant being located near the 250 m isobaths north of the Bjørnøya and Hopen troughs (Fig. 1b) (Loeng, 1991). During the winter months of the sampling year 2001, south and west coast of Spitsbergen were regularly covered by drift ice (Fig. 2).

2.3 Modern depositional environment

The sedimentary environments of the sample locations have been characterised by sea floor photographs taken with the Remotely Operated Vehicle (ROV “sprint 103”) (Fig. 3) (Winkelmann and Knies, 2005). The environments are classified into three different settings: (A) a high energy-no accumulation environment on the outer shelf/shelf

CPD

9, 4145–4189, 2013

A new ice-rafted debris provenance proxy

A. Müller and J. Knies

Title Page

Abstract

Introduction

Conclusions

References

Tables

Figures

◀

▶

◀

▶

Back

Close

Full Screen / Esc

Printer-friendly Version

Interactive Discussion



A new ice-rafted debris provenance proxy

A. Müller and J. Knies

Title Page

Abstract

Introduction

Conclusions

References

Tables

Figures



Back

Close

Full Screen / Esc

Printer-friendly Version

Interactive Discussion



break and bathymetric highs, (B) a low energy-high accumulation environment in the inner fjords and (C) a mixed type of moderate or variable energy-low accumulation environment of the transitional sites and the Barents Sea. Especially the winnowed lag deposits on the outer shelf (Setting A) are considered to represent erosional surfaces probably induced by contour or bottom currents (Andrulleit et al., 1996). The “ice-rafted debris (IRD) – signal” of these hard ground surfaces may not reflect recent ice rafting but out washing of finer sediments. The onset of increased along-shelf bottom currents was dated to approximately 2.6 kyr BP (Andrulleit et al., 1996). The winnowing facies is observed on the shelf to water depth > 130 m bsf west off Prins Karls Forland. Towards the incisions of the fjord systems (Setting B), areas are sheltered from the bottom currents and therefore sites favouring deposition of modern ice-rafting. In contrast, the sediments from the Barents Sea shelf exhibit partly features of the higher energetic shelf environments west off Spitsbergen (Setting C). Within the Atlantic water domain, strong bottom currents ($\sim 0.5 \text{ ms}^{-1}$, based on ROV observation) leave single ice rafted boulder outstanding. However, resuspension, entrainment and lateral displacement of fine grained sediments seem to be not as dominant as on the shelf west off Spitsbergen.

3 Materials

3.1 Offshore samples

9 short cores (length 30 cm, diameter 11 cm) have been collected west off Svalbard and on the adjacent shelf to the south on a scientific cruise with RV *Heincke* in summer 2001 (Fig. 1b). The short cores were taken with multicorer equipment. Undisturbed surfaces of all short cores (the upper first centimetre of the cores) were sampled and stored at -20°C until analysis. Thereafter, all samples were freeze-dried and washed through > 500 μm mesh with deionized water. 198 detrital quartz grains up to 3 mm in diameter were hand-picked from the > 500 μm size fraction and embedded in epoxide

resin and polished down half size for SEM and LA-ICP-MS analysis. The 198 grains represent all quartz grains > 500 µm found in the available sample material. Samples were selected from two respective environmental settings (Table 1) including fossil ice rafting (> 2.6 kyr) (Setting A) and modern ice rafting (Setting B). Samples from the outer Barents Sea shelf (Setting C) have not been studied.

3.2 Onshore samples

18 representative samples from Svalbard including 4 quartzites, 2 hydrothermal quartz veins, 2 conglomerates, and 10 sandstones from potential provenance areas in central, west, south and southeast Spitsbergen were studied in order to compare the quartz CL structures, micro and chemistry with quartz grains of offshore samples (Fig. 1b, Table 2). The samples originate from archives of the Geological Survey of Norway (NGU) in Trondheim, University Centre in Svalbard (UNIS) CO₂ Lab AS in Longyearbyen, the Norwegian Polar Institute (NPI) in Tromsø, and the Store Norske Spitsbergen Grubekompani (SNSG) AS. Additional samples were collected during field work at Edgeøya in summer 2012 by colleagues from NGU and the UNIS CO₂ Lab AS.

4 Methods

Mineral inclusions and intergrowths of non-quartz minerals occurring in some of the quartz grains were identified by optical microscopy and BSE imaging and were semi-quantitatively analysed using the LEO 1450VP SEM equipped with EDX-detector at the Geological Survey of Norway in Trondheim. Different quartz populations and intra-granular micro structures such as growth zoning, healed fractures, authigenic quartz overgrowths, were imaged using a Centaurus BS Bialkali type CL detector attached to the SEM.

LA-ICP-MS was applied for the in situ determination of the elements Li, Be, Mn, Ge, Al, Ti, and Fe in 133 out of 198 quartz grains. 65 grains were not analysed due to the

CPD

9, 4145–4189, 2013

A new ice-rafted debris provenance proxy

A. Müller and J. Knies

Title Page

Abstract

Introduction

Conclusions

References

Tables

Figures

⏪

⏩

◀

▶

Back

Close

Full Screen / Esc

Printer-friendly Version

Interactive Discussion



high number of mineral and/or fluid inclusions which would contaminate the analyses. The ICP-MS used in this study is a double focusing sector field instrument (ELEMENT-1 Finnigan MAT) combined with a New Wave UP-193-nm excimer laser probe. Continuous raster ablation was carried out, resulting in ablated rasters of approximately 150 μm \times 100 μm with depths of 20 to 30 μm . Element concentrations were calculated by multi-standard calibration. Limits of detection (LOD) are listed in Tables A1 and B1. The analytical error ranges within 10% of the absolute concentration of the element. Detailed description of the measurement procedures are given by Flem et al. (2002) and Flem and Müller (2012).

5 Results

5.1 Characteristics of quartz grains in offshore samples

The quartz grains of offshore samples were classified into five major types, A to E, based on mineral micro inclusions, CL intensity, intra-granular structures visualised by SEM-CL imaging and trace element content (Fig. 4). The characteristics of the five types are distinctive and can be described as follows.

Type A comprises monocrystalline, sub- to well-rounded, mineral-inclusion-free quartz grains (0.4 to 1.4 mm) with no or very low CL signal. Type A grains are almost ubiquitous in every sampling area and form the major grain population (mean 48%) of nearly all the samples except samples 1265 (Isfjord) and 1269 (Forland-sund; Figs. 4, 5). A number of these grains show cemented sericite and traces of Fe-oxides/hydroxides at their surfaces which are highlighted by black arrows in Fig. 4. These coatings represent remains of cement from eroded sandstone and, thus, the A type grains are detrital quartz grains from eroded sandstones (secondary origin) (Table 3). The primary sources of the grains, before sedimentation as sandstones, were low-grade metamorphic quartzites and/or low-temperature hydrothermal segregations, facilitating the CL properties according to Bernet and Bassett (2005). Type

A new ice-rafted debris provenance proxy

A. Müller and J. Knies

Title Page

Abstract

Introduction

Conclusions

References

Tables

Figures



Back

Close

Full Screen / Esc

Printer-friendly Version

Interactive Discussion



A new ice-rafted debris provenance proxy

A. Müller and J. Knies

[Title Page](#)[Abstract](#)[Introduction](#)[Conclusions](#)[References](#)[Tables](#)[Figures](#)[◀](#)[▶](#)[◀](#)[▶](#)[Back](#)[Close](#)[Full Screen / Esc](#)[Printer-friendly Version](#)[Interactive Discussion](#)

A quartz commonly has low Ti ($< 2.9 \mu\text{g g}^{-1}$), low Li ($\leq 1.8 \mu\text{g g}^{-1}$), and variable Al (< 8 to $221 \mu\text{g g}^{-1}$; Table A1). Exceptions are three grains containing high Li (mean $110 \mu\text{g g}^{-1}$) and Al (mean $2762 \mu\text{g g}^{-1}$) (Fig. 6). Such high Li and Al concentrations have been described from hydrothermal quartz only (e.g. Jourdan et al., 2009). Ti concentrations $< 2.9 \mu\text{g g}^{-1}$ indicate quartz crystallisation temperatures $< 450^\circ\text{C}$ (Wark and Watson, 2006) implying low-grade metamorphic and hydrothermal primary origin of A-type grains (Table 3).

Type B grains are polycrystalline and polyphase quartz grains (0.6 to 3 mm) with no or very low CL signal. The quartz is intergrown with K-feldspar, mica (biotite and/or muscovite), chlorite, and calcite and contains micro inclusions of apatite, pyrite, Fe oxides, calcite, dolomite, barite, rutile, zircon, and monazite. The group comprises 28 % of the investigated grains. Type B grains are shown as BSE images in Fig. 4 in order to visualise their polyphase compositions. The quartz has low Ti ($< 2.9 \mu\text{g g}^{-1}$), low Li ($\leq 2.8 \mu\text{g g}^{-1}$), and variable Al (< 8 to $344 \mu\text{g g}^{-1}$). The element concentrations are in the same range as for type A grains (Fig. 6). Like the type A grains, type B grains show microcrystalline remains of sericite and Fe-oxides/hydroxides on the grain surfaces (see black arrows in Fig. 4) indicating that they are detrital grains from eroded sandstones (secondary origin). The primary sources of the type B grains are low-grade metamorphic quartzites (Table 3).

Type C represents a distinct quartz population comprising 7 % of the grains investigated. The non-luminescent grains (0.6 to 1.2 mm) are cut by thin, healed, brightly luminescent micro-fractures. Single grains of this type were found in almost all the sampled regions except Isfjord. Coatings of sericite and Fe-oxides/hydroxides at the grain surfaces (see black arrow in Fig. 4) indicate that type C grains represent detrital grains from eroded sandstones (secondary origin) similar to type A and B grains. Type C grains have a consistent trace element content characterised by low Li (mean $1.4 \mu\text{g g}^{-1}$) and moderate Al (mean $149 \mu\text{g g}^{-1}$; Fig. 6). The CL properties and the trace element signature suggest that the type C grains are primarily erosion products of

low-grade metamorphic quartzites and/or hydrothermal segregations or veins (primary origin) which were deposited in sandstones (Table 3).

Type D grains comprising 14 % of the investigated samples are polycrystalline quartz fragments (0.5 to 1.5 mm) consisting of rounded to well-rounded, partially broken detrital quartz grains with remains of authigenic quartz (see white arrows in Fig. 4). The detrital grains commonly have bright CL and authigenic quartz is non-luminescent. The pore space of the sandstone fragments is completely filled by authigenic quartz. These fragments occur predominantly in Isfjord and to a lesser extent in Storfjord, Prins Karls Forland, Van Mijenfjord and Forlandsund. The majority of the detrital grains shows thin (< 5 µm), healed and non-luminescent micro-fractures which are characteristic of high-grade metamorphic and plutonic origin (e.g. Seyedolali et al., 1997). Moderate to high Ti concentrations (9.1 to 182.9 µg g⁻¹; Fig. 6) indicate minimum crystallisation temperatures of the detrital quartz from 523 ± 9 to 825 ± 14 °C (Wark and Watson, 2006), confirming the plutonic or high-grade metamorphic primary origin of the detrital quartz grains. The monomineralic composition of the type D fragments and complete silicification of the pore space suggest that they originate from mature, coarse-grained sandstones (secondary origin, Table 3).

Type E grains comprise fine-grained arkose fragments (2 to 3 mm) containing predominantly detrital rounded quartz grains and some K-feldspar grains cemented by non-luminescent authigenic quartz. Most of the detrital quartz grains exhibit moderate to bright CL intensity indicating plutonic or high-grade metamorphic primary origins. Type E is represented by four grains, found only in sample 1244 from inner Storfjord.

5.2 Characteristics of quartz grains in onshore samples

For comparison quartz grains in onshore rocks including sandstones, conglomerates, quartzites and hydrothermal quartz veins from the Brøgger peninsula, St. Jonsfjord, Kongsfjord, Billefjord, Edgeøya, Isfjord, and Lunckefjell were analysed (Table 2). The sample locations are indicated in Fig. 1b and their stratigraphic origins are shown in Fig. 7.

CPD

9, 4145–4189, 2013

A new ice-rafted debris provenance proxy

A. Müller and J. Knies

Title Page

Abstract

Introduction

Conclusions

References

Tables

Figures



Back

Close

Full Screen / Esc

Printer-friendly Version

Interactive Discussion



A new ice-rafted debris provenance proxy

A. Müller and J. Knies

Title Page

Abstract

Introduction

Conclusions

References

Tables

Figures



Back

Close

Full Screen / Esc

Printer-friendly Version

Interactive Discussion

The Proterozoic and Permo-Carboniferous onshore samples from the *Brøgger peninsula*, *St. Jonsfjord* and *Kongsfjord* are located in the glacier ice and river catchment areas of the northern Forlandsund, relatively close to the offshore sample locations 1268, 1269, and 1286. The quartz CL structures of the majority of these samples are different to those of the offshore grains. Quartz of samples 84–132, 31–50, YO85-269 and WS79-8 has distinctive, lamella-like structures in CL (Fig. 8a) and quartz in sample YO-193 shows cloudy domains of bright luminescence within dull luminescent quartz (Fig. 8b). Samples YO85-Årat consists of quartz with moderate intense CL cross-cut by thin ($< 5 \mu\text{m}$), healed micro-fractures with bright CL similar to type C grains (Fig. 8c). However, the CL intensity and the Ti content ($5.2 \mu\text{g g}^{-1}$; Table B1) of the YO85-Årat quartz are significantly higher than that of the offshore type C grains. The sandstone and conglomerate of the Permo-Carboniferous Gipsdalen Group at St. Jonsfjord (WS87-4, WS87-25) contain 10 to 15 % dull luminescent, feature-less quartz grains corresponding type A and 80 to 85 % bright luminescent quartz grains with non-luminescent, healed micro-fractures similar to type D grains (Fig. 8d, e). The detrital grains are cemented by dull-luminescent authigenic quartz. However, the secondary structures of the type-D-like grains are more common in grains of the Gipsdalen sediments than in the offshore grains (compare Figs. 4 and 8d). Concentrations of Al, Ti and Li plot in the same range as the offshore samples (Fig. 9). However, the proportion of grains with $\text{Ti} > 2.9 \mu\text{g g}^{-1}$ (42 %) is significantly higher than in most of the offshore samples (Fig. 9a).

Sample MJ2 is a chert pebble from the Permo-Carboniferous Gipsdalen Group at *Billefjord* close to offshore sample 1265 in the Isfjord. Chert is a common constituent of the Permo-Carboniferous sediments of Spitsbergen. In CL the sample shows a brecciated, moderate bright luminescent chert generation which is healed by a dull luminescent chert generation (Fig. 8f). Such structures have not been observed in the offshore grains. The chert has variable Al ($81 \pm 63 \mu\text{g g}^{-1}$), high Fe (mean $28 \pm 7 \mu\text{g g}^{-1}$) and no Ti (Table B1).

A new ice-rafted debris provenance proxy

A. Müller and J. Knies

Title Page

Abstract

Introduction

Conclusions

References

Tables

Figures



Back

Close

Full Screen / Esc

Printer-friendly Version

Interactive Discussion



Four medium-grained sandstones (AB12-4, AB12-16, PO1, PO2) from two different stratigraphic units of the Late Triassic De Geerdalen Formation at *Edgeøya* were investigated. All sandstones are moderately sorted, containing 80–85 % sub-angular quartz grains with an average grain size of $\sim 180 \mu\text{m}$ (AB12-4, AB12-16) and $\sim 120 \mu\text{m}$ (PO1, PO2), respectively (Fig. 10a). The cement consists of sericite, authigenic quartz and minor Fe oxides/hydroxides. Small (5 to $100 \mu\text{m}$), euhedral authigenic quartz crystals occur in the interspace of the porous sandstone. The *Edgeøya* sandstones contain principally four types of quartz grains: (1) grains with dull, feature-less CL corresponding type A grains (47 to 64 %), (2) grains with dull, feature-less CL and polyphase micro inclusions mostly mica similar to type B grains (10 to 18 %) (Fig. 10b), (3) dull luminescent grains with cross-cutting bright luminescent veins similar to type C grains (1 to 4 %), and (4) grains with bright CL and superimposing non-luminescent secondary structures corresponding type D grains (27 to 34 %). Thus, the sandstones of the De Geerdalen Formation consist of the same quartz grain populations as most of the offshore samples. Even the grain type proportions of the *Egdeøya* sandstone and some offshore samples are comparable (1258, 1286; 1275, 1276) (Fig. 5).

Samples DH-4, DH7A-1, DH7A-2, DH7A-3 are representative medium- to coarse-grained Mesozoic sandstones from southern *Isfjord* (Table 2, Fig. 7). Mesozoic sediments cover about 30 % of SW Spitsbergen (Fig. 1b). All sandstones are badly sorted with sericite cement. The sub-angular to rounded quartz grains comprise 80 to 100 % of the grains in the sediments. Authigenic quartz is not developed. Between 13 and 50 % of the quartz grains exhibit feature-less CL with weak intensity corresponding the CL characteristics of type A grains. The other population comprises quartz grains with bright CL superimposed by dull luminescent thin ($< 5 \mu\text{m}$) veins corresponding type D grains (Fig. 10c). The bright luminescent type D grains are characterized by high and variable average Ti of $76 \pm 80 \mu\text{g g}^{-1}$ (Table B1; Fig. 9c). Sample DH7A-1 is the only investigated onshore sample which contains fragments of fine-grained arkose which correspond to type E grains (Fig. 10d). Type B and C grains were not found.

The conglomerate MJ1 is a representative sample of the Tertiary Van Mijenfjorden Group from *Lunckefjell*. Tertiary sediments cover about 30% of SW Spitsbergen (Fig. 1b). Large quartz grains (> 1 mm) are sub-rounded and small grains are sub-angular. The grains are cemented by weak luminescent authigenic quartz (Fig. 10e). 61% of the quartz grains have bright CL corresponding the CL characteristics of type D grains. The other quartz grains have feature-less CL with low intensity similar to type A grains. In addition, a few grains of chert were identified (Fig. 10f).

6 Discussion

A- and B-type grains are ubiquitous in almost all offshore regions sampled and represent the major quartz-grain populations in the > 500 µm size fraction (Figs. 4, 5). The homogeneity in frequency and regional distribution of the two grain populations suggests that the onshore rocks close to the offshore sampling sites do not serve as the main catchment areas. The onshore lithologies close to the offshore sample locations are either Proterozoic crystalline rocks (Oscar II Land east of Forlandsund, eastern Prins Karls Forland), Palaeozoic metamorphic rocks (western Prins Karls Forland), or Mesozoic to Cenozoic sedimentary rocks (Van Mijenfjord, Isfjord and Storfjord) (Dallmann et al., 2002). The erosion of rocks of such diverse sedimentary and metamorphic histories would produce quartz grains with highly variable trace element concentrations and CL properties. Indeed, all investigated onshore samples east of Forlandsund contain quartz with CL features that are completely absent in the offshore grains (Fig. 8a–c). Further, different from the offshore grains type D quartz grains are the most dominant quartz population in all investigated sandstones north and south of Isfjord. Only in the innermost Isfjord (sample 1265) close to the glacier ice and river catchment areas, significant proportion of type D quartz grains occurs in the > 500 µm fraction. It implies that modern ice rafting in the Forlandsund area cannot be the result of local iceberg melting.

A new ice-rafted debris provenance proxy

A. Müller and J. Knies

Title Page

Abstract

Introduction

Conclusions

References

Tables

Figures



Back

Close

Full Screen / Esc

Printer-friendly Version

Interactive Discussion



A new ice-rafted debris provenance proxy

A. Müller and J. Knies

Title Page

Abstract

Introduction

Conclusions

References

Tables

Figures

⏪

⏩

◀

▶

Back

Close

Full Screen / Esc

Printer-friendly Version

Interactive Discussion

Similar frequency and prevalence of type A and B quartz grains are observed in Setting A (“fossil ice rafting”) locations 1275 and 1276 outside Prins Karls Forland as well (Figs. 3, 5). These winnowed lag deposits are widely distributed on the shelf in water depth > 130 m (Winkelmann and Knies, 2005). The IRD most likely represents a mixture of debris released by melting sea-ice and icebergs prior to 2.6 kyr (Andrulleit et al., 1996). The prevalence of type A and B grains in these “fossil” sediments suggest the same source for the quartz grains as for the modern ice-rafted material. It confirms the hypothesis that the onshore rocks close to the offshore sampling sites are not the main source, and, thus, that the main catchment area is somewhere else.

Similar circumstances are postulated for type C grains. These occur in almost all sampled regions except Isfjord but form, in contrast to type A and B grains, a minor grain population. However, it appears that types A, B and C grains are regionally and genetically connected. The three types are recycled grains of immature sandstones, which originally were eroded from a low-grade metamorphic province with quartzites and low-temperature quartz segregations. Immature sandstones are common in the Mesozoic and Tertiary sedimentary successions of southeast and east Spitsbergen (Storfjord area, Barentsøya, Edgeøya and Hopen) (Dallmann, 1999). In fact, the quartz populations and their proportions identified in the Late Triassic sandstones of the De Geerdalen Formation from Edgeøya resemble closest to the populations and their distributions found in most of the offshore samples. The similarities of the grain types occurring in the offshore samples and onshore samples from Edgeøya are astonishing as illustrated in Fig. 11. Thus, it is suggested that most of the IRD origin from these sediments which are exposed at Edgeøya, Barentsøya, Hopen and along the coast of inner Storfjorden. In order to further confirm this source area of the type A, B and C grains, the ice drift will be considered below.

IRD of all grain sizes are transported predominantly by icebergs calved from the margins of tidewater glaciers, and to a much lesser extent by sea ice (Barnes et al., 1982; Nürnberg et al., 1994; Bischof, 2001). Icebergs and sea ice, and any included debris, drift under the action of ocean currents up to several hundred kilometres (Elverhøi

A new ice-rafted debris provenance proxy

A. Müller and J. Knies

Title Page

Abstract

Introduction

Conclusions

References

Tables

Figures



Back

Close

Full Screen / Esc

Printer-friendly Version

Interactive Discussion

et al., 1995; Hebbeln et al., 1998) and, to a lesser extent, wind. The drift ice melts and releases the debris, whereby coarser-grained material ($> 500 \mu\text{m}$ size fraction) falls directly to the sea floor. The transport of drift ice in the sampling area is controlled by the East Spitsbergen Current (ESC; e.g. Loeng, 1991; Fig. 1b). Entering the Barents Sea from the east/northeast the ESC turns into Storfjord and continues encircling southern Spitsbergen where it flows northward along the continental shelf, passing Forland-sund and Prins Karls Forland. Occasionally westerly winds blow drift ice coming with the ESC in the inner parts of the fjords along the western coast, namely Hornsund, Van Mijenfjord, Isfjord and Kongsfjord (Umbreit, 2009), implying that even the sample sites 1258 and 1265 might be affected by ESC drift ice. The major sources of icebergs in the catchment area of the ESC are fast moving (surging) tidewater glaciers at the east coast of Edgeøya and in inner Storfjord (Dowdeswell and Dowdeswell, 1997; Figs. 1b, 2). A number of smaller tidewater glaciers occur along the east coast of Spitsbergen between 77° and 78° N. However, calving icebergs hardly reach the west coast of Spitsbergen today. More important is the Storfjord area as the main producer of sea ice in southern Spitsbergen (Nilsen and Gammelsrød, 2008; Fig. 2). Sea ice is predominantly ($> 50\%$) formed in open water areas. However, ca.30% of the ice is produced as fast or pack ice (Haarpaintner et al., 2001) where sediments from the Edgeøya and Barentsøya can be incorporated and eventually transported via ESC towards the Spitsbergen west coast and further around the S cape northward.

Thus, the most likely regional sources of the IRD for type A, B, and C are the east coast of Edgeøya and Barentsøya and the inner Storfjord (Fig. 5). The dominant lithology in the catchment area of the tidewater glaciers are sediments of the Triassic Kapp Toscana Group and Sassendalen Group (Dallmann, 1999; Dallmann et al., 2002). The up to 400 m thick De Geerdalen Formation, part of the Kapp Toscana Group, is the most widespread sandstone-rich succession exposed in the suggested catchment areas of Edgeøya and inner Storfjorden. Summarizing, the type A, B and C grains are recycled detrital grains of immature sandstone with sericite-Fe-oxide/hydroxide coatings which

commonly occur in the Triassic De Geerdalen Formation at Edgeøya, Barentsøya and inner Storfjord, south Spitsbergen.

The type D grains are fragments of mature sandstones containing detrital grains of high-grade metamorphic and plutonic origins cemented by authigenic quartz. They are very different from the type A, B, and C grains. The fragments occur as minor constituents in the samples from Storfjord, Van Mijenfjord, Forlandsund and Prins Karls Forland but they are the major constituent in the sample from the inner Isfjord. Thus, the type D grains in the Isfjord sample 1265 represent a local source (Fig. 5). Type D grains are the dominant grain population in sandstones of the Kapp Toscana and Adventdalen Group in the vicinity of the location of sample 1265. Tidewater glaciers of the Tempelfjord and – in historical times – Sassendal are the major source of drift ice in inner Isfjord (cf. Forwick and Vorren, 2009) (Fig. 1b). The rock units in the catchment area of these glaciers include sediments of these formations.

The type E arkose grains, which occur only in sample 1244 from inner Storfjord are undoubtedly a local contribution from nearby onshore rocks. The sampling site is close to the mouth of the Agardhdal. The sedimentary sequences around Agardhdal comprise among others the Early Cretaceous Adventdalen Group (Dallmann et al., 1999). The investigated sandstone DH7A-1 of the Helvetiafjellet Formation within the Adventdalen Group is the only onshore sample in which type E grains were found (Fig. 11). The Helvetiafjellet Formation lies in the glacier and river catchment area of the Agardhdal close to the offshore sample (Fig. 1) and it is the likely source for the type E grains found in sample 1244.

7 Implications and conclusions

The identification of geological provinces by means of IRD-derived quartz grains (> 500 µm) in marine sediments off the Spitsbergen coast provides a new dimension in terms of reconstructing the dynamics and extent of past Spitsbergen/Barents Sea ice-sheet drainage basins. Traditionally, the configuration of the Weichselian ice sheets

CPD

9, 4145–4189, 2013

A new ice-rafted debris provenance proxy

A. Müller and J. Knies

Title Page

Abstract

Introduction

Conclusions

References

Tables

Figures



Back

Close

Full Screen / Esc

Printer-friendly Version

Interactive Discussion



A new ice-rafted debris provenance proxy

A. Müller and J. Knies

Title Page

Abstract

Introduction

Conclusions

References

Tables

Figures



Back

Close

Full Screen / Esc

Printer-friendly Version

Interactive Discussion



in the Spitsbergen/Barents Sea region is reconstructed by combining evidence from terrestrial sediment and landforms with marine IRD records (cf. Svendsen et al., 2004). The intensity of IRD supply is thereby both indicative for the timing of maximal extent and break-up of the ice sheet (Knies et al., 2001; Jessen et al., 2010). Provenance studies on bulk material further constrain the sources of glacially eroded material, but can add little information on the regional dynamics of past ice sheet configurations (Vogt et al., 2001; Tütken et al., 2002; Moros et al., 2006; Andrews et al., 2009). The latter may be inferred from the imagery of submarine landforms in the Barents Sea (Dowdeswell et al., 2010; Winsborrow et al., 2010), but configurations of previous glaciations remain unresolved unless applying 3-D seismic technology (Laberg et al., 2010).

Our data demonstrate that the descriptive CL characteristics of detrital quartz in combination with quantitative trace element determination by LA-ICP-MS provide a useful tool for the classification of the IRD grains into populations of distinctive provenance on Spitsbergen. Given a larger regional set of surface and downcore samples this source specific information from IRD-derived quartz grains may help to improve the reconstruction of ice-drainage patterns by identifying prominent zones of glacial erosion, not only during the late Weichselian but possibly during previous glaciations as well. So far, we have identified five distinct quartz grain populations (types A to E) in sediments off the Spitsbergen coast, indicative of potential IRD provinces in the Storfjord area.

The ubiquity of type A and B grains indicates a common regional source. They are recycled detrital grains of immature sandstone with sericite cement of a kind which commonly occurs in the Triassic De Geerdalen Formation on Edgeøy, Barentsøya and in inner Storfjord. The less common type C grains are genetically related to type A and B grains. All three grain populations have been identified in onshore sandstones of the Late Triassic De Geerdalen Formation which are likely the source of these quartz grains. Type D grains are fragments of mature, silicified, coarse-grained sandstones containing detrital quartz grains of primary high-grade metamorphic and plutonic origin. Type D grains form a minor constituent in a number of samples representing local

sources that are presumably silicified mature sandstones. Type E grains occurring only in inner Storfjord, are arkose fragments presumably originating from the Early Cretaceous Adventdalen Group.

The results imply that under modern (interglacial) conditions IRD deposition along the southern and western Spitsbergen margin is mainly governed by ESC-controlled ice drift patterns (mainly sea-ice). The presence of detrital quartz from local provinces however, indicates that variations in IRD supply from western and southern Spitsbergen may be quantified as well. In summary, applying this new IRD proxy on Arctic continental margin sediments will allow better definition of the sources of IRD and, thus, spatial and temporal changes of ice flow drainage patterns during glacial and deglacial periods.

Acknowledgements. We highly appreciate the logistic help of Per Terje Osmundsen and Jan Sverre Sandstad from the Geological Survey of Norway in Trondheim, Synnøve Elvevold from the Norwegian Polar Institute in Tromsø, and colleagues from the University Centre in Svalbard CO₂ Lab AS and Store Norske Spitsbergen Grubekompani AS who provided the onshore samples from Spitsbergen and Egdeøya. We greatly appreciate improvement of the English text by R. Boyd.

References

- Andrews, J. T., Darby, D., Eberle, D., Jennings, A. E., Moros, M., and Ogilvie, A.: A robust, multisite Holocene history of drift ice off northern Iceland: implications for North Atlantic climate, *Holocene*, 19, 71–77, 2009.
- Andruleit, H., Freiwald, A., and Schafer, P.: Bioclastic carbonate sediments on the southwestern Svalbard shelf, *Mar. Geol.*, 134, 163–182, 1996.
- Barnes, P. W., Reimnitz, E., and Fox, D.: Ice rafting of fine-grained sediment, a sorting and transport mechanism, Beaufort Sea, Alaska, *J. Sediment. Petrol.*, 52, 493–502, 1982.
- Bernet, M. and Bassett K.: Provenance analysis by single-quartz-grain SEM-CL/optical microscopy, *J. Sediment. Res.*, 75, 492–500, 2005.

A new ice-rafted debris provenance proxy

A. Müller and J. Knies

Title Page

Abstract

Introduction

Conclusions

References

Tables

Figures

◀

▶

◀

▶

Back

Close

Full Screen / Esc

Printer-friendly Version

Interactive Discussion



A new ice-rafted debris provenance proxy

A. Müller and J. Knies

[Title Page](#)[Abstract](#)[Introduction](#)[Conclusions](#)[References](#)[Tables](#)[Figures](#)[Back](#)[Close](#)[Full Screen / Esc](#)[Printer-friendly Version](#)[Interactive Discussion](#)

- Bischof, J.: Ice drift, ocean circulation and climate change, Springer, Heidelberg, Germany, 2001.
- Bjørlykke, K. and Elverhøi, A.: Reworking of Mesozoic clayey material in the north-western part of the Barents Sea, *Mar. Geol.*, 18, M29–M34, 1975.
- 5 Dallmann, W. K. (Ed.): Lithostratigraphic Lexicon of Svalbard, Review and Recommendations for Nomenclature Use, Late Palaeozoic to Quaternary Bedrock, Norwegian Polar Institute, Norway, 1999.
- Dallmann, W. K., Ohta, Y., Elvevold, S., and Blomeier, D. (Eds.): Bedrock Map of Svalbard and Jan Mayen, Norsk Polarinstituttemakart No. 33, 2002.
- 10 Darby, D. A., Bischof, J. F., Spielhagen, R. F., Marshall, S. A., and Herman, S. W.: Arctic ice export events and their potential impact on global climate during the late Pleistocene, *Paleoceanography*, 17, 1025, doi:10.1029/2001PA000639, 2002.
- Dibner, V. D., Basov, V. A., Gerke, A. A., Solovyeva, M. F., Sisopatrova, G. P., and Shulgina, N. I.: The age of the re-Quaternary deposits on the bottom of the Barents Sea, *Oceanology*, 10, 520–529, 1970.
- 15 Dowdeswell, J. A. and Dowdeswell, E. K.: Modern glaciers and climate change, in: *Geology of Svalbard: Geol. Soc. Memoir*, 17, edited by: Harland, W. B., 436–445, 1997.
- Dowdeswell, J. A., Hogan, K. A., Evans, J., Noormets, R., Cofaigh, C. Ó, and Ottesen, D.: Past ice-sheet flow east of Svalbard inferred from streamlined subglacial landforms, *Geology*, 38, 163–166, 2010.
- 20 Elverhøi, A., Andersen, E. S., Dokken, T., Hebbeln, D., Spielhagen, R., Svendsen, J. I., Sorflaten, M., Rornes, A., Hald, M., and Forsberg, C. F.: The growth and decay of the late weichselian ice sheet in western Svalbard and adjacent areas based on provenance studies of marine sediments, *Quaternary Res.*, 44, 303–316, 1995.
- 25 Flem, B. and Müller, A.: In situ analysis of trace elements in quartz using laser ablation inductively coupled plasma mass spectrometry, in: *Quartz: Deposits, Mineralogy and Analyt-ics*, edited by: Götze, J. and Möckel, R., Springer, Berlin, Heidelberg, Germany, 219–236, doi:10.1007/978-3-642-22161-3_10, 2012.
- Flem, B., Larsen, R. B., Grimstedt, A., and Mansfeld, J.: In situ analysis of trace elements in quartz by using laser ablation inductively coupled plasma mass spectrometry, *Chem. Geol.*, 182, 237–247, doi:10.1016/S0009-2541(01)00292-3, 2002.
- 30 Forwick, M. and Vorren, T. O.: Late Weichselian and Holocene sedimentary environments and ice rafting in Isfjorden, Spitsbergen, *Paleogeogr. Paleocl.*, 280, 258–274, 2009.

A new ice-rafted debris provenance proxy

A. Müller and J. Knies

Title Page

Abstract

Introduction

Conclusions

References

Tables

Figures



Back

Close

Full Screen / Esc

Printer-friendly Version

Interactive Discussion



Götze, J.: Chemistry, textures and physical properties of quartz – geological interpretation and technical application, *Mineral. Mag.*, 73, 645–671, doi:10.1180/minmag.2009.073.4.645, 2009.

Götze, J. and Zimmerle, W.: Quartz and Silica as Guide to Provenance in Sediments and Sedimentary Rocks, *Contr. Sediment. Geol.*, 21, Schweizerbart'sche Verlagsbuchhandlung, Stuttgart, Germany, 2000.

Grousset, F. E., Labeyrie, L., Sinko, J. A., Cremer, M., Bond, G., Duprat, J., Cortijo, E., and Huon, S.: Patterns of ice-rafted detritus in the glacial north Atlantic (40–55° N), *Paleoceanography*, 8, 175–192, 1993.

Haarpaintner, J., Gascard, J. C., and Haugan, P. M.: Ice production and brine formation in Storfjorden, Svalbard, *J. Geophys. Res.-Oceans*, 106, 14001–14013, 2001.

Harland, W. B. (Ed.): *Geology of Svalbard*, *Geol. Soc. Memoir*, 17, 1997.

Hebbeln, D., Henrich, R., and Baumann, K. H.: Paleocyanography of the last interglacial/glacial cycle in the Polar North Atlantic, *Quaternary Sci. Rev.*, 17, 125–153, 1998.

Hemming, S. R.: Heinrich events: massive late Pleistocene detritus layers of the North Atlantic and their global climate imprint, *Rev. Geophys.*, 42, RG1005, doi:10.1029/2003RG000128, 2004.

Jessen, S. P., Rasmussen, T. L., Nielsen, T., and Solheim, A.: A new Late Weichselian and Holocene marine chronology for the western Svalbard slope 30 000e0 cal years BP, *Quaternary Sci. Rev.*, 29, 1301–1312, 2010.

Jourdan, A.-L., Vennemann, T. W., Mullis, J., Ramseyer, K., and Spiers, C. J.: Evidence of growth and sector zoning in hydrothermal quartz from Alpine veins, *Eur. J. Mineral.*, 21, 219–231, 2009.

Knies, J., Kleiber, H. P., Matthiessen, J., Muller, C., and Nowaczyk, N.: Marine ice-rafted debris records constrain maximum extent of Saalian and Weichselian ice-sheets along the northern Eurasian margin, *Global Planet. Change*, 31, 45–64, 2001.

Laberg, J. S., Andreassen, K., Knies, J., Vorren, T. O., and Winsborrow, M.: Late Pliocene-Pleistocene development of the Barents Sea ice sheet, *Geology*, 38, 107–110, 2010.

Lang Farmer, G., Barber, D., and Andrews, J.: Provenance of Late Quaternary ice-proximal sediments in the North Atlantic: Nd, Sr and Pb isotopic evidence, *Earth Planet. Sc. Lett.*, 209, 227–243, 2003.

Loeng, H.: Features of the physical oceanographic conditions of the Barents Sea, *Polar Res.*, 10, 5–18, 1991.

A new ice-rafted debris provenance proxy

A. Müller and J. Knies

Title Page

Abstract

Introduction

Conclusions

References

Tables

Figures

◀

▶

◀

▶

Back

Close

Full Screen / Esc

Printer-friendly Version

Interactive Discussion



- Michelsen, J. K. and Khorasani, G. K.: A regional study on coals from Svalbard: organic facies, maturity and thermal history, *B. Soc. Geol. Fr.*, 162, 385–397, 1991.
- Moros, M., Andrews, J. T., Eberl, D. D., and Jansen, E.: Holocene history of drift ice in the northern North Atlantic: evidence for different spatial and temporal modes, *Paleoceanography*, 21, PA2017, doi:10.1029/2005PA001214, 2006.
- Müller, A. and Koch-Müller, M.: Hydrogen speciation and trace element contents of igneous, hydrothermal and metamorphic quartz from Norway, *Mineral. Mag.*, 73, 569–583, doi:10.1180/minmag.2009.073.4.569, 2009.
- Nilsen, F. and Gammelsrød, T.: Large sea ice production affects the climate?, *The University Centre in Svalbard News*, available at: http://www.unis.no/60_NEWS/6040_Archive_2008/n_08_06_04_storfjorden/Storfjorden_news_04062008.htm (last access: 8 November 2008), 2008.
- Nørgaard-Pedersen, N., Spielhagen, R. F., Thiede, J., and Kassens, H.: Central Arctic surface ocean environment during the past 80 000 years, *Paleoceanography*, 13, 193–204, 1998.
- Nürnberg, D., Wolkenburg, I., Dethleff, D., Eicken, H., Kassens, H., Letzig, T., Reimnitz, E., and Thiede, J.: Sediments in Arctic sea ice: implications for entrainment, transport and release, *Mar. Geol.*, 119, 185–214, 1994.
- Peck, V. L., Halla, I. R., Zahn, R., Grousset, F., Hemming, S. R., and Scourse, J. D.: The relationship of Heinrich events and their European precursors over the past 60 kyr BP: a multi-proxy ice-rafted debris provenance study in the North East Atlantic, *Quaternary Sci. Rev.*, 26, 862–875, 2007.
- Schlichtholz, P. and Goszczko, I.: Interannual variability of the Atlantic water layer in the West Spitsbergen Current at 76.5° N in summer 1991–2003, *Deep-Sea Res.*, 53, 608–626, 2006.
- Seyedolali, A., Krinsley D. H., Boggs, S., O’Hara, P. F., Dypvik, H., and Goles, G. G.: Provenance interpretation of quartz by scanning electron microscope – cathodoluminescence fabric analysis, *Geology*, 25, 787–790, 1997.
- Skogseth, R.: Dense Water Production Processes in Storfjorden, Report No.2-2003, University Center on Svalbard, Longyearbyen, Norway, 2003.
- Steel, R. J. and Worsley, D.: Svalbard’s post-Caledonian strata: an atlas of sedimentational patterns and palaeogeographic evolution, in: *Petroleum Geology of the North European Margin*, edited by: Spencer, A. M., Holter, E., Johnsen, S. O., Mørk, A., Nysæther, E., Songstad, P., and Spinnangr, Å., Graham and Trotman, London, UK, 109–135, 1984.

A new ice-rafted debris provenance proxy

A. Müller and J. Knies

Title Page

Abstract

Introduction

Conclusions

References

Tables

Figures

◀

▶

◀

▶

Back

Close

Full Screen / Esc

Printer-friendly Version

Interactive Discussion



Sundvor, E.: Seismic refraction and reflection measurements in the southern Barents Sea, *Mar. Geol.*, 16, 255–273, 1974.

Svendsen, J. I., Alexanderson, H., Astakhov, V. I., Demidov, I., Dowdeswell, J. A., Funder, S., Gataullin, V., Henriksen, M., Hjort, C., Houmark-Nielsen, M., Hubberten, H. W., Ingolfsson, O., Jakobsson, M., Kjaer, K. H., Larsen, E., Lokrantz, H., Lunkka, J. P., Lysa, A., Mangerud, J., Matiouchkov, A., Murray, A., Moller, P., Niessen, F., Nikolskaya, O., Polyak, L., Saarnisto, M., Siegert, C., Siegert, M. J., Spielhagen, R. F., and Stein, R.: Late quaternary ice sheet history of northern Eurasia, *Quaternary Sci. Rev.*, 23, 1229–1271, 2004.

Tütken, T., Eisenhauer, A., Wiegand, B., and Hansen, B. T.: Glacial-interglacial cycles in Sr and Nd isotopic composition of Arctic marine sediments triggered by the Svalbard/Barents Sea ice sheet, *Mar. Geol.*, 182, 351–372, 2002.

Umbreit, A.: Spitzbergen, Conrad Stein Verlag, Kiel, Germany, 2009.

Verplanck, E. V., Lang Farmer, G., Andrews, J., Gita Dunhill, G., and Millo, C.: Provenance of Quaternary glacial and glacial-marine sediments along the southeast Greenland margin, *Earth Planet. Sci. Lett.*, 286, 52–62, 2009.

Vogt, C., Knies, J., Spielhagen, R. F., and Stein, R.: Detailed mineralogical evidence for two nearly identical glacial/deglacial cycles and Atlantic water advection to the Arctic Ocean during the last 90 000 years, *Global Planet. Change*, 31, 23–44, 2001.

Wark, D. A. and Watson, E. B.: TitaniQ: a titanium-in-quartz geothermometer, *Contr. Mineral. Petrol.*, 152, 743–754, 2006.

Winkelmann, D. and Knies, J.: Recent distribution and accumulation of organic carbon on the continental margin west off Spitsbergen, *Geochem. Geophys. Geosys.*, 6, Q09012, doi:10.1029/2005GC000916, 2005.

Winsborrow, M. C. M., Andreassen, K., Corner, G. D., and Laberg, J. S.: Deglaciation of a marine-based ice sheet: Late Weichselian palaeo-ice dynamics and retreat in the southern Barents Sea reconstructed from onshore and offshore glacial geomorphology, *Quaternary Sci. Rev.*, 29, 424–442, 2010.

A new ice-rafted debris provenance proxy

A. Müller and J. Knies

Table 1. Studied sea-floor samples and environmental settings (see text for definition). The number of grains represent all quartz grains $> 500 \mu\text{m}$ which were found and investigated by optical microscopy, BSE and SEM-CL imaging. The numbers in parentheses indicate the number of LA-ICP-MS analyses.

Sample	Latitude [N]	Longitude [E]	Water Depth [m]	Setting	No. of Grains
1244	77° 56'	19° 09'	96	B	14 (4)
1246	76° 46'	19° 25'	153	B	16 (8)
1258	77° 49'	15° 45'	43	B	24 (13)
1265	78° 22'	16° 22'	87	B	8 (5)
1268	78° 37'	11° 38'	102	B	12 (11)
1269	78° 22'	12° 19'	169	B	14 (10)
1275	78° 15'	10° 10'	297	A	32 (17)
1276	78° 33'	10° 19'	131	A	34 (27)
1286	78° 52'	11° 19'	159	B	44 (38)

Title Page

Abstract

Introduction

Conclusions

References

Tables

Figures

◀

▶

◀

▶

Back

Close

Full Screen / Esc

Printer-friendly Version

Interactive Discussion



Table 2. Origin and type of investigated onshore samples for comparative studies. NGU – Geological Survey of Norway in Trondheim, NPI – Norwegian Polar Institute in Tromsø, SNSG – Store Norske Spitsbergen Grubekompani AS, UNIS CO₂ Lab – University Centre in Svalbard CO₂ Lab AS, Fm – Formation.

Sample	Rock type	Area	Geological unit	Age	Latitude [N]	Longitude [E]	Sample archive
YO85-269	quartzite	Brøgger peninsula	Kongsvegen Group	Mesoproterozoikum	78° 52′	12° 06′	NPI
YO85-193	quartzite	Brøgger peninsula	Kongsvegen Group	Mesoproterozoikum	78° 52′	12° 06′	NPI
YO85-Årat	quartzite	Brøgger peninsula	Kongsvegen Group	Mesoproterozoikum	78° 52′	12° 06′	NPI
84-132	hydrothermal vein quartz in biotite schist	Kongsfjord	Krossfjorden Group	Mesoproterozoikum	79° 04′	12° 16′	NGU
31-50	hydrothermal vein quartz in biotite schist	Kongsfjord	Krossfjorden Group	Mesoproterozoikum	79° 04′	12° 16′	NGU
WS79-8	metagranite	Vestkysten	?	Neoproterozoic?	78° 35′	12° 19′	NPI
WS87-4	conglomerate	St. Jonsfjord	Gipsdalen Group	Late Carboniferous to Early Permian	78° 32′	13° 16′	NPI
WS87-25	sandstone	St. Jonsfjord	Gipsdalen Group	Late Carboniferous to Early Permian	78° 29′	13° 24′	NPI
MJ2	chert pebble	Billefjord (N Isfjord)	Gipsdalen Group Holtberget Fm	Late Carboniferous to Early Permian	78° 29′	15° 57′	SNSG
AB12-4	sandstone	Edgeøya	Kapp Toscana Group De Geerdalen Fm	Late Triassic	77° 27′	20° 50′	UNIS CO ₂ Lab
AB12-16	sandstone	Edgeøya	Kapp Toscana Group De Geerdalen Fm	Late Triassic	77° 27′	20° 57′	UNIS CO ₂ Lab
PO1	sandstone	Edgeøya	Kapp Toscana Group De Geerdalen Fm	Late Triassic	77° 26′	20° 52′	NGU
PO2	sandstone	Edgeøya	Kapp Toscana Group De Geerdalen Fm	Late Triassic	77° 26′	20° 52′	NGU
DH4	sandstone	S Isfjord	Kapp Toscana Group Knorringsfjellet Fm	Late Triassic to Early Jurassic	78° 12′	15° 49′	UNIS CO ₂ Lab
DH7A-1	sandstone	S Isfjord	Adventdalen Group Helvetiafjellet Fm	Early Cretaceous	78° 12′	15° 49′	UNIS CO ₂ Lab
DH7A-2	sandstone	S Isfjord	Adventdalen Group Helvetiafjellet Fm	Early Cretaceous	78° 12′	15° 49′	UNIS CO ₂ Lab
DH7A-3	sandstone	S Isfjord	Adventdalen Group Carolinefjellet Fm	Early Cretaceous	78° 12′	15° 49′	UNIS CO ₂ Lab
MJ1	conglomerate	Lunckefjell	Van Mijenfjorden Group Firkanten Fm	Tertiary	78° 00′	16° 51′	SNSG

A new ice-rafted debris provenance proxy

A. Müller and J. Knies

Title Page

Abstract

Introduction

Conclusions

References

Tables

Figures



Back

Close

Full Screen / Esc

Printer-friendly Version

Interactive Discussion



A new ice-rafted debris provenance proxy

A. Müller and J. Knies

[Title Page](#)

[Abstract](#)

[Introduction](#)

[Conclusions](#)

[References](#)

[Tables](#)

[Figures](#)

⏪

⏩

◀

▶

[Back](#)

[Close](#)

[Full Screen / Esc](#)

[Printer-friendly Version](#)

[Interactive Discussion](#)

Table 3. Suggested primary and secondary rock type origin of quartz grains in the > 500 μm fraction of investigated offshore samples.

Grain type	Primary origin (prior to sedimentation as sandstone of Carboniferous to Tertiary age)	Secondary origin (prior to Pleistocene to recent marine sedimentation)
A	low-grade metamorphic quartzites and/or hydrothermal segregations	immature sandstones cemented by sericite and Fe-oxides/hydroxides
B	low-grade metamorphic quartzites	immature sandstones cemented by sericite and Fe-oxides/hydroxides
C	low-grade metamorphic quartzites and/or hydrothermal segregations	immature sandstones cemented by sericite and Fe-oxides/hydroxides
D	plutonic or high-grade metamorphic rocks	mature sandstones cemented by authigenic quartz
E	plutonic or high-grade metamorphic rocks	arkose cemented by authigenic quartz

Table A1. Trace element concentrations of quartz grains (type A to E) in offshore samples determined by LA-ICP-MS. Concentrations of B, P, and K are below the limits of detection (LOD) of 3.3, 4.6 and 25.4 $\mu\text{g g}^{-1}$, respectively.

sample	LOD type	Li 0.31	Be 0.06	Mn 0.10	Ge 0.14	Al 8.1	Ti 2.9	Fe 1.5
1244-B-A	A	<0.31	0.08	0.16	1.55	31.9	<2.9	2.2
1244-B-B	A	0.39	0.08	0.84	1.00	89.9	<2.9	190.4
1244-A-C	E	0.54	<0.08	1.33	0.94	33.2	5.7	2.5
1244-B-A	A	0.75	0.09	5.07	<0.14	68.2	<2.9	56.8
1246-A-A	A	<0.31	<0.06	0.31	1.49	<8.1	<2.9	31.5
1246-A-B	A	<0.31	<0.06	0.22	1.26	<8.1	<2.9	1.5
1246-A-C	A	<0.31	<0.06	0.28	1.17	10.5	<2.9	<1.5
1246-B-A	A	0.96	<0.06	0.97	1.02	127.7	<2.9	9.9
1246-B-B	B	<0.31	0.09	0.45	0.85	46.6	3.1	3.8
1246-B-C	A	0.75	<0.06	1.75	1.02	202.6	<2.9	84.6
1246-B-D	B	0.47	0.16	1.02	1.61	42.9	3.3	6.8
1246-B-E	A	0.98	<0.06	1.48	1.09	221.5	<2.9	20.3
1258-A-A	D	0.78	<0.06	0.35	0.95	76.9	81.8	84.4
1258-A-B	A	0.18	0.11	0.06	1.18	<8.1	<2.9	3.7
1258-A-C	D	2.62	<0.06	1.03	1.02	42.5	22.7	17.6
1258-A-D	A	0.50	<0.06	1.04	1.05	16.7	<2.9	<1.5
1258-A-E	A	<0.31	<0.06	0.35	0.96	13.1	<2.9	<1.5
1258-B-F	B	1.44	0.14	0.26	2.40	335.0	<2.9	124.3
1258-B-G	D	13.44	0.08	1.75	1.42	406.5	49.6	90.9
1258-B-H	B	2.60	<0.06	0.27	1.90	285.1	<2.9	38.0
1258-B-I	B	<0.31	<0.06	1.77	1.33	65.7	<2.9	23.2
1258-B-J	B	<0.31	<0.06	0.50	1.42	47.4	<2.9	3.4
1258-B-K	D	3.58	1.22	3.20	0.76	221.0	28.0	4.8
1258-B-L	B	2.80	0.17	0.47	2.71	344.9	<2.9	97.7
1258-B-M	D	0.79	0.15	4.02	0.50	43.8	44.9	15.4

A new ice-rafted debris provenance proxy

A. Müller and J. Knies

Title Page

Abstract

Introduction

Conclusions

References

Tables

Figures

⏪

⏩

◀

▶

Back

Close

Full Screen / Esc

Printer-friendly Version

Interactive Discussion



Table A1. Continued.

sample	LO type	Li 0.31	Be 0.06	Mn 0.10	Ge 0.14	Al 8.1	Ti 2.9	Fe 1.5
1265-B-A	D	0.47	0.11	0.51	< 0.14	257.6	88.5	9.4
1265-B-B	D	0.44	< 0.06	0.39	0.73	85.3	64.6	10.8
1265-B-C	D	1.01	0.06	11.98	0.83	306.3	182.9	216.0
1265-B-D	D	0.63	< 0.06	4.42	0.89	116.7	111.2	108.2
1265-B-E	D	< 0.31	< 0.06	7.35	0.68	47.3	179.9	231.6
1268-A-A	A	< 0.31	< 0.06	0.20	0.24	13.6	< 2.9	< 1.5
1268-A-B	A	< 0.31	< 0.06	0.10	0.31	28.9	< 2.9	1.4
1268-A-C	A	< 0.31	< 0.06	0.12	0.22	22.5	< 2.9	7.2
1268-A-D	A	< 0.31	< 0.06	0.18	0.21	15.3	< 2.9	< 1.5
1268-B-A	C	2.45	0.20	3.04	0.70	166.0	< 2.9	27.5
1268-B-B	A	< 0.31	0.14	0.15	1.77	78.9	< 2.9	< 1.5
1268-B-C	C	1.39	< 0.06	0.74	2.41	235.7	< 2.9	21.7
1268-B-D	A	< 0.31	< 0.06	0.58	1.94	184.4	< 2.9	< 1.5
1268-B-E	C	2.55	< 0.06	0.79	4.49	344.1	< 2.9	57.5
1268-B-F	A	0.79	0.14	0.10	1.76	21.2	< 2.9	< 1.5
1268-B-G	A	< 0.31	0.13	0.20	1.98	125.0	< 2.9	1.7
1269-A-A	D	0.62	< 0.06	0.43	0.92	70.2	26.8	16.4
1269-A-B	B	0.32	0.27	6.08	0.97	134.	< 2.9	20.7
1269-A-C	B	0.58	0.27	7.15	0.84	51.4	< 2.9	15.6
1269-A-D	A	< 0.31	< 0.06	39.59	1.55	52.6	< 2.9	122.0
1269-A-E	A	< 0.31	0.19	15.01	1.83	28.1	< 2.9	101.5
1269-A-F	B	< 0.31	< 0.06	2.19	0.96	91.6	< 2.9	34.2
1269-A-G	A	< 0.31	< 0.06	18.35	1.85	32.4	< 2.9	38.4
1269-A-H	B	0.33	< 0.06	0.20	1.44	33.5	< 2.9	6.1
1269-A-I	B	0.52	0.29	1.17	1.02	48.6	< 2.9	3.7
1269-A-J	B	< 0.31	0.13	0.31	0.98	20.6	< 2.9	5.8

A new ice-rafted debris provenance proxy

A. Müller and J. Knies

Title Page

Abstract

Introduction

Conclusions

References

Tables

Figures

⏪

⏩

◀

▶

Back

Close

Full Screen / Esc

Printer-friendly Version

Interactive Discussion



A new ice-rafted debris provenance proxy

A. Müller and J. Knies

Title Page

Abstract

Introduction

Conclusions

References

Tables

Figures



Back

Close

Full Screen / Esc

Printer-friendly Version

Interactive Discussion



Table A1. Continued.

sample	LO type	Li 0.31	Be 0.06	Mn 0.10	Ge 0.14	Al 8.1	Ti 2.9	Fe 1.5
1275-A-A	A	< 0.31	0.11	0.46	1.54	56.1	< 2.9	1.6
1275-A-B	A	130.44	0.24	0.35	8.17	3555.4	< 2.9	9.1
1275-A-C	A	< 0.31	< 0.06	0.45	1.04	19.9	< 2.9	11.3
1275-A-D	A	< 0.31	0.17	0.59	< 0.14	32.6	< 2.9	5.7
1275-A-E	A	171.27	0.38	0.21	5.03	2245.8	< 2.9	17.7
1275-A-F	A	29.07	0.19	0.12	5.91	2485.4	< 2.9	6.6
1275-B-A	A	0.77	< 0.06	0.30	0.57	32.6	4.0	16.7
1275-B-B	B	< 0.31	< 0.06	3.43	1.01	106.4	< 2.9	82.8
1275-B-C	A	3.37	< 0.06	0.17	1.66	148.5	< 2.9	170.2
1275-B-D	A	1.32	< 0.06	0.73	0.68	22.4	4.7	105.9
1275-B-E	A	2.95	0.11	0.21	1.23	190.4	< 2.9	17.2
1275-B-F	C	0.44	< 0.06	0.56	1.58	72.4	< 2.9	11.3
1275-B-G	C	< 0.31	< 0.06	0.45	1.61	47.3	< 2.9	5.2
1275-B-H	A	1.78	< 0.06	< 0.10	1.24	158.4	< 2.9	7.1
1275-B-I	B	< 0.31	0.09	0.14	2.12	43.6	< 2.9	1.8
1275-B-J	C	1.11	< 0.06	0.38	1.55	41.3	< 2.9	5.6
1275-B-K	B	< 0.31	0.15	0.31	2.08	40.5	< 2.9	< 1.4

Table A1. Continued.

sample	LO type	Li 0.31	Be 0.06	Mn 0.10	Ge 0.14	Al 8.1	Ti 2.9	Fe 1.5
1276-A3-A	D	2.53	0.18	1.04	1.31	178.9	39.33	9.7
1276-A3-B	D	3.34	0.35	1.18	1.04	118.4	46.7	3.1
1276-A3-C	D	17.71	0.83	0.99	0.81	340.6	48.4	4.6
1276-A3-D	A	< 0.31	< 0.06	1.21	0.37	47.6	< 2.9	10.6
1276-A3-E	A	< 0.31	0.10	0.48	0.37	98.4	< 2.9	104.3
1276-A3-F	D	3.14	0.12	1.56	< 0.1	146.1	34.3	7.6
1276-A3-G	A	< 0.31	< 0.06	0.67	0.29	40.9	< 2.9	4.1
1276-A3-H	A	< 0.31	0.26	1.07	0.21	62.8	< 2.9	9.6
1276-A3-I	A	< 0.31	< 0.06	0.35	0.83	9.5	< 2.9	< 1.5
1276-A3-J	A	< 0.31	< 0.06	0.23	1.06	10.6	< 2.9	< 1.5
1276-A3-K	D	23.92	0.48	1.02	0.69	327.0	53.8	4.0
1276-A3-L	D	2.70	< 0.06	0.56	1.21	181.1	33.7	5.8
1276-A3-M	D	21.14	0.29	0.74	0.63	205.6	45.8	1.7
1276-A3-N	D	12.94	1.00	1.27	0.73	414.5	57.3	8.0
1276-B-A	B	1.37	< 0.06	0.23	1.85	75.0	< 2.9	12.9
1276-B-B	B	0.81	< 0.06	0.57	1.60	127.2	< 2.9	220.2
1276-B-C	B	< 0.31	< 0.06	0.52	0.28	< 8.1	< 2.9	< 1.5
1276-B-D	E	< 0.31	< 0.06	0.40	0.69	151.0	18.5	15.8
1276-B-E	B	< 0.31	< 0.06	0.77	0.15	26.0	< 2.9	5.3
1276-B-F	A	0.33	< 0.06	0.30	0.94	104.9	< 2.9	28.9
1276-B-G	A	0.49	< 0.06	0.26	1.15	41.5	< 2.9	2.6
1276-B-H	E	0.47	< 0.06	0.50	0.79	124.9	11.7	7.4
1276-B-I	D	0.64	< 0.06	0.58	0.99	101.5	9.1	< 1.5
1276-B-J	B	0.34	< 0.06	7.11	0.14	8.5	< 2.9	43.0
1276-B-K	A	< 0.31	< 0.06	0.86	2.38	100.4	< 2.9	5.8
1276-B-L	D	< 0.31	< 0.06	0.34	0.57	183.4	17.4	128.7
1276-B-M	B	< 0.31	< 0.06	0.34	0.55	22.9	< 2.9	2.4

A new ice-rafted debris provenance proxy

A. Müller and J. Knies

Title Page

Abstract

Introduction

Conclusions

References

Tables

Figures



Back

Close

Full Screen / Esc

Printer-friendly Version

Interactive Discussion



A new ice-rafted debris provenance proxy

A. Müller and J. Knies

Title Page

Abstract

Introduction

Conclusions

References

Tables

Figures

⏪

⏩

◀

▶

Back

Close

Full Screen / Esc

Printer-friendly Version

Interactive Discussion



Table A1. Continued.

sample	LO type	Li 0.31	Be 0.06	Mn 0.10	Ge 0.14	Al 8.1	Ti 2.9	Fe 1.5
1286-A1-A	B	1.79	< 0.06	0.44	1.13	30.6	< 2.9	< 1.5
1286-A1-B	B	1.80	0.64	0.27	1.07	21.9	< 2.9	2.4
1286-A1-C	B	0.32	< 0.06	0.21	0.88	59.3	< 2.9	14.0
1286-A1-D	B	0.37	< 0.06	0.21	1.04	23.4	3.2	1.7
1286-A2-A	A	< 0.31	< 0.06	0.26	0.78	27.5	< 2.9	13.7
1286-A2-B	A	< 0.31	< 0.06	0.31	0.85	28.8	< 2.9	< 1.5
1286-A2-C	B	< 0.31	< 0.06	0.20	0.79	24.0	10.4	17.5
1286-A2-D	B	0.52	0.07	1.54	0.81	111.8	12.3	98.4
1286-A2-E	A	< 0.31	0.22	0.22	1.39	21.8	< 2.9	5.9
1286-A2-F	A	< 0.31	0.13	0.25	1.40	11.9	< 2.9	2.2
1286-A2-G	B	< 0.31	< 0.06	10.79	1.08	136.3	< 2.9	< 32.5
1286-A2-H	A	0.31	0.54	< 0.10	1.48	21.1	< 2.9	2.0
1286-B-A	C	1.48	< 0.06	0.37	1.40	136.5	< 2.9	5.7
1286-B-A	D	0.41	< 0.06	0.13	0.57	28.2	28.5	< 1.5
1286-B-B	B	< 0.31	0.10	0.21	1.26	43.0	< 2.9	2.5
1286-B-C	B	< 0.31	< 0.06	0.21	1.28	59.6	< 2.9	< 1.5
1286-B-D	B	< 0.31	< 0.06	< 0.10	1.33	47.1	< 2.9	1.5
1286-B-E	B	< 0.31	< 0.06	< 0.10	1.42	35.5	< 2.9	4.2
1286-B-F	A	< 0.31	< 0.06	0.24	1.03	63.9	< 2.9	46.0
1286-B-G	A	< 0.31	0.11	0.27	0.99	51.8	< 2.9	24.2
1286-B-H	A	< 0.31	< 0.06	0.35	0.40	45.6	< 2.9	35.7
1286-B-I	B	< 0.31	0.10	0.20	1.15	48.3	< 2.9	18.6
1286-B-J	B	< 0.31	< 0.06	0.16	1.13	42.7	< 2.9	1.8

A new ice-rafted debris provenance proxy

A. Müller and J. Knies

Title Page

Abstract

Introduction

Conclusions

References

Tables

Figures



Back

Close

Full Screen / Esc

Printer-friendly Version

Interactive Discussion



Table A1. Continued.

sample	LO type	Li 0.31	Be 0.06	Mn 0.10	Ge 0.14	Al 8.1	Ti 2.9	Fe 1.5
1286-B-K	A	0.38	< 0.06	0.42	< 0.14	29.1	< 2.9	< 1.5
1286-B-L	A	1.36	< 0.06	0.36	0.20	36.1	< 2.9	< 1.5
1286-B-M	A	1.14	< 0.06	0.50	< 0.14	48.6	< 2.9	< 1.5
1286-B-N	A	< 0.31	< 0.06	0.39	1.13	45.7	< 2.9	4.4
1286-B-O	A	< 0.31	< 0.06	0.41	1.03	29.4	< 2.9	13.5
1286-B-P	A	< 0.31	< 0.06	0.14	1.29	14.3	< 2.9	< 1.5
1286-B-Q	A	0.49	< 0.06	0.15	1.38	9.1	< 2.9	< 1.5
1286-B-R	A	< 0.31	< 0.06	0.21	1.13	< 8.1	< 2.9	< 1.5
1286-B-S	A	< 0.31	< 0.06	0.30	1.16	13.0	< 2.9	1.8
1286-B-T	A	0.36	< 0.06	0.40	1.42	< 8.1	< 2.9	< 1.5
1286-B-U	A	< 0.31	< 0.06	< 0.10	1.87	31.6	< 2.9	1.9
1286-B-V	A	< 0.31	< 0.06	0.20	1.81	34.5	< 2.9	3.7
1286-B-W	A	< 0.31	0.10	0.22	1.90	34.6	< 2.9	3.6
1286-B-X	A	< 0.31	0.21	0.24	1.25	10.2	< 2.9	1.5
1286-B-Y	A	< 0.31	< 0.06	0.37	1.17	11.5	< 2.9	1.5

A new ice-rafted debris provenance proxy

A. Müller and J. Knies

Title Page

Abstract

Introduction

Conclusions

References

Tables

Figures

◀

▶

◀

▶

Back

Close

Full Screen / Esc

Printer-friendly Version

Interactive Discussion



Table B1. Trace element concentrations of quartz in onshore samples determined by LA-ICP-MS. Concentrations of B, P, and K are below the limits of detection (LOD) of 3.3, 4.6 and 25.4 $\mu\text{g g}^{-1}$, respectively. Type A, B, C, and D correspond to quartz grain types found in offshore sediments (see text for explanation). Type X quartz was not found in offshore sediments.

sample	LO type	Li 0.31	Be 0.06	Mn 0.10	Ge 0.14	Al 8.1	Ti 2.9	Fe 1.5
84-132-A	X	3.22	< 0.06	0.22	1.03	26.6	4.0	< 1.5
84-132-B	X	3.87	< 0.06	0.06	1.48	7.7	< 2.9	< 1.5
31-50-A	X	1.81	0.09	0.37	1.02	19.1	< 2.9	< 1.5
31-50-B	X	0.55	0.28	< 0.10	0.64	26.0	< 2.9	< 1.5
YO85-269-A	X	3.12	0.13	0.33	0.85	56.4	< 2.9	5.3
YO85-269-B	X	0.46	0.16	0.42	1.14	14.3	< 2.9	< 1.5
YO85-193	X	0.36	0.25	0.15	2.11	12.2	< 2.9	< 1.5
YO85-Årat	X	0.61	0.18	0.46	0.16	77.0	5.2	20.2
WS79-8-A	X	0.58	< 0.06	0.15	0.81	16.8	< 2.9	< 1.5
WS79-8-B	X	0.87	< 0.06	0.25	1.06	25.5	3.5	< 1.5
WS87-4-A	A	1.44	< 0.06	< 0.10	1.02	126.0	< 2.9	2.2
WS87-4-B	D	11.68	0.11	0.60	1.73	272.1	144.0	42.6
WS87-25-A	D	2.25	0.15	0.33	0.66	359.4	19.3	20.7
WS87-25-B	D	< 0.31	< 0.06	< 0.10	0.45	382.5	23.4	53.3
MJ2-A	X	0.32	0.06	0.74	0.70	77.1	< 2.9	36.2
MJ2-B	X	< 0.31	< 0.06	0.30	0.88	20.0	< 2.9	22.7
MJ2-C	X	< 0.31	0.28	0.42	1.05	145.4	< 2.9	25.2

A new ice-rafted debris provenance proxy

A. Müller and J. Knies

Title Page

Abstract

Introduction

Conclusions

References

Tables

Figures

⏪

⏩

◀

▶

Back

Close

Full Screen / Esc

Printer-friendly Version

Interactive Discussion



Table B1. Continued.

sample	LO type	Li 0.31	Be 0.06	Mn 0.10	Ge 0.14	Al 8.1	Ti 2.9	Fe 1.5
AB12-4-A	A	< 0.31	< 0.06	0.12	0.24	23.1	< 2.9	4.5
AB12-4-B	A	0.66	< 0.06	0.24	0.22	42.5	< 2.9	< 1.5
AB12-4-C	D	0.47	0.11	0.21	< 0.14	188.1	68.1	< 1.5
AB12-4-D	D	0.44	< 0.06	0.42	0.73	97.1	74.0	6.4
AB12-4-E	D	1.01	0.06	1.97	0.63	196.2	112.2	16.1
AB12-4-F	B	< 0.31	< 0.06	0.69	1.85	65.0	< 2.9	2.7
AB12-4-G	D	0.63	< 0.06	0.42	1.09	95.5	82.1	18.0
AB12-4-H	D	< 0.31	< 0.06	4.38	0.78	87.1	122.9	1.6
AB12-4-I	A	< 0.31	< 0.06	0.12	0.31	18.2	< 2.9	1.4
AB12-4-J	A	< 0.31	< 0.06	0.31	0.21	35.1	< 2.9	< 1.5
AB12-4-K	C	< 0.31	< 0.06	0.37	1.26	45.0	< 2.9	3.7
AB12-4-L	B	0.61	< 0.06	0.17	0.15	36.0	< 2.9	2.5
DH4-A	D	1.85	0.21	0.48	1.20	23.0	12.9	< 1.5
DH4-B	D	0.88	< 0.06	0.59	0.64	99.7	108.1	7.2
DH4-C	A	< 0.31	< 0.06	0.20	0.80	10.1	< 2.9	< 1.5
DH4-D	A	0.75	< 0.06	< 0.10	0.51	< 8.1	< 2.9	2.2
DH4-E	A	< 0.31	0.09	0.78	0.54	10.7	< 2.9	1.6

A new ice-rafted debris provenance proxy

A. Müller and J. Knies

Title Page

Abstract

Introduction

Conclusions

References

Tables

Figures

⏪

⏩

◀

▶

Back

Close

Full Screen / Esc

Printer-friendly Version

Interactive Discussion



Table B1. Continued.

sample	LO type	Li 0.31	Be 0.06	Mn 0.10	Ge 0.14	Al 8.1	Ti 2.9	Fe 1.5
DH7A-1-A	D	0.86	< 0.06	0.32	0.61	43.6	14.92	5.2
DH7A-1-B	D	2.67	0.30	0.90	1.52	302.9	35.70	6.7
DH7A-1-C	D	1.29	< 0.06	0.48	0.96	15.4	14.86	< 1.5
DH7A-1-D	D	1.41	< 0.06	0.20	0.58	66.2	221.07	42.2
DH7A-1-E	D	3.06	< 0.06	0.37	0.82	58.6	47.99	2.2
DH7A-1-F	D	2.03	< 0.06	0.54	0.91	179.9	40.94	12.4
DH7A-1-G	D	< 0.31	< 0.06	0.30	0.41	< 8.1	8.66	< 1.5
DH7A-1-H	D	2.18	< 0.06	0.27	0.60	35.2	47.75	1.8
DH7A-1-I	D	1.38	0.08	0.76	0.83	57.2	25.24	3.2
DH7A-1-J	D	1.49	< 0.06	0.26	0.73	87.3	35.47	3.9
DH7A-1-K	D	4.28	0.07	1.43	0.63	213.4	287.84	78.5
DH7A-2-A	D	1.48	< 0.06	0.71	0.62	125.3	144.07	91.4
DH7A-2-B	D	1.36	< 0.06	0.88	1.84	159.5	24.47	44.2
DH7A-3-A	D	0.65	< 0.06	0.47	0.70	112.6	145.39	66.2
DH7A-3-B	D	2.75	0.96	< 0.10	0.73	46.0	68.93	7.8
MJ1-A	A	0.95	< 0.06	0.19	0.97	13.4	< 2.9	< 1.5
MJ1-B	A	1.92	< 0.06	0.29	0.80	< 8.1	< 2.9	< 1.5
MJ1-C	D	3.93	< 0.06	0.43	2.11	42.2	13.8	< 1.5
MJ1-D	D	2.95	0.26	0.18	1.95	32.4	12.1	< 1.5

A new ice-rafted debris provenance proxy

A. Müller and J. Knies

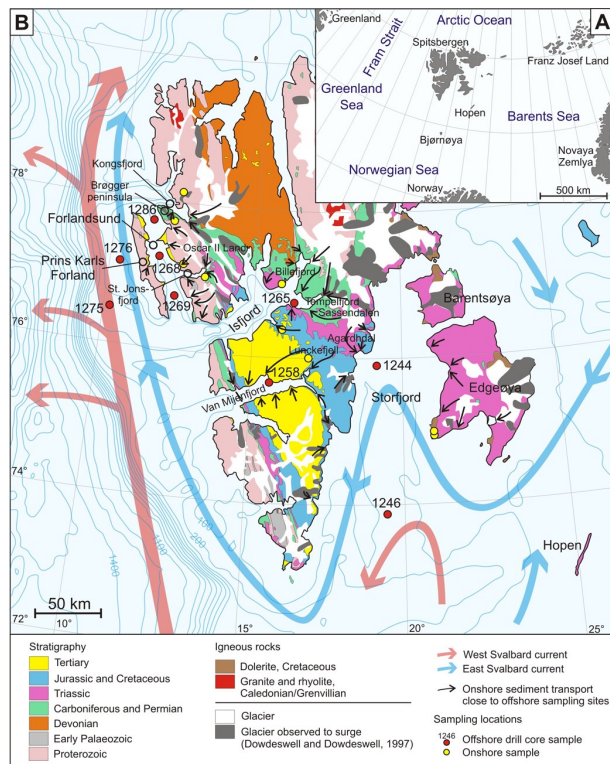


Fig. 1. (A) – Location of Spitsbergen between the Greenland Sea, Barents Sea, Norwegian Sea and Arctic Ocean. **(B)** – Simplified geological map of Spitsbergen according to Dallmann et al. (2002) with locations of offshore drill core samples (red dots) and onshore rock samples (yellow dots) and onshore sediment transport close to offshore sample locations (small black arrows). In addition, the map shows the East and West Spitsbergen Current and the distribution of surging glaciers according to Dowdeswell and Dowdeswell (1997).

Title Page

Abstract

Introduction

Conclusions

References

Tables

Figures

◀

▶

◀

▶

Back

Close

Full Screen / Esc

Printer-friendly Version

Interactive Discussion



A new ice-rafted debris provenance proxy

A. Müller and J. Knies

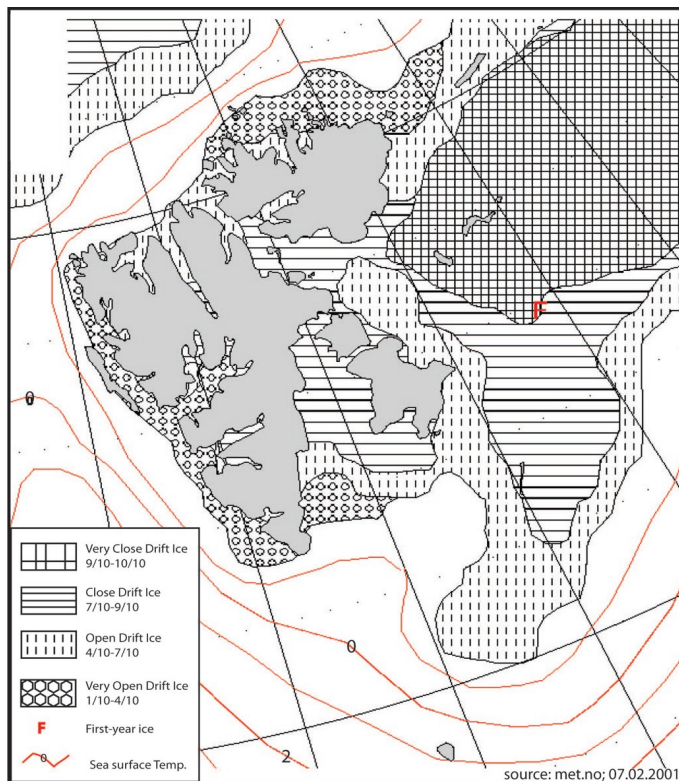
[Title Page](#)[Abstract](#)[Introduction](#)[Conclusions](#)[References](#)[Tables](#)[Figures](#)[Back](#)[Close](#)[Full Screen / Esc](#)[Printer-friendly Version](#)[Interactive Discussion](#)

Fig. 2. Sea ice conditions around Spitsbergen on 7 February 2001, the year when the offshore drill core samples were taken (source: www.met.no).

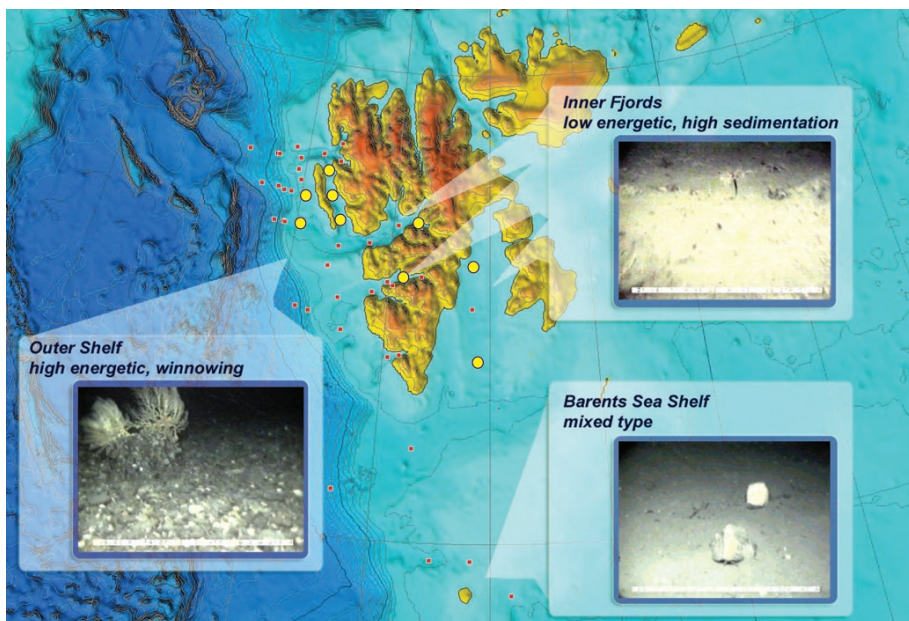


Fig. 3. Three types of sedimentary environment (modified after Winkelmann and Knies, 2005): **(A)** outer shelf, high energetic – no sedimentation; **(B)** inner fjords, low energetic – high sedimentation; **(C)** Barents Sea shelf, mixed type of medium energetic – low sedimentation (based on interpretation of ROV pictures). Yellow dots indicate the studied core-top samples. The small red squares mark samples studied by Winkelmann and Knies (2005).

A new ice-rafted debris provenance proxy

A. Müller and J. Knies

Title Page

Abstract

Introduction

Conclusions

References

Tables

Figures



Back

Close

Full Screen / Esc

Printer-friendly Version

Interactive Discussion



	core	Type A CL image	Type B BSE image	Type C CL image	Type D CL image	Type E CL image
Storfjord	1244					
	43	14	14	29		
Van Mijenfjord	1246					
	38	38	24			
Isfjord	1258					
	42	33	8	17		
Forlandsund	1265					
	1269					
	43	57				
Prins Karls Forland	1268					
	66	17	17			
	1286					
Prins Karls Forland	1275					
	56	32	6	6		
Prins Karls Forland	1276					
	42	35		23		

Fig. 4. Classification of quartz grains of the > 500 μm size fraction according to their CL characteristics and micro inclusion contents. Representative CL images of type A, C, D and E grains and BSE images of type B grains are shown. The numbers in the lower left of each cell indicate the percentage on the total number of quartz grains found. The scale bar length corresponds to 200 μm . The black arrows indicate remains of sericite cement at quartz grain edges and the white arrows remains of authigenic quartz.

A new ice-rafted debris provenance proxy

A. Müller and J. Knies

Title Page

Abstract

Introduction

Conclusions

References

Tables

Figures

⏪

⏩

◀

▶

Back

Close

Full Screen / Esc

Printer-friendly Version

Interactive Discussion



A new ice-rafted debris provenance proxy

A. Müller and J. Knies

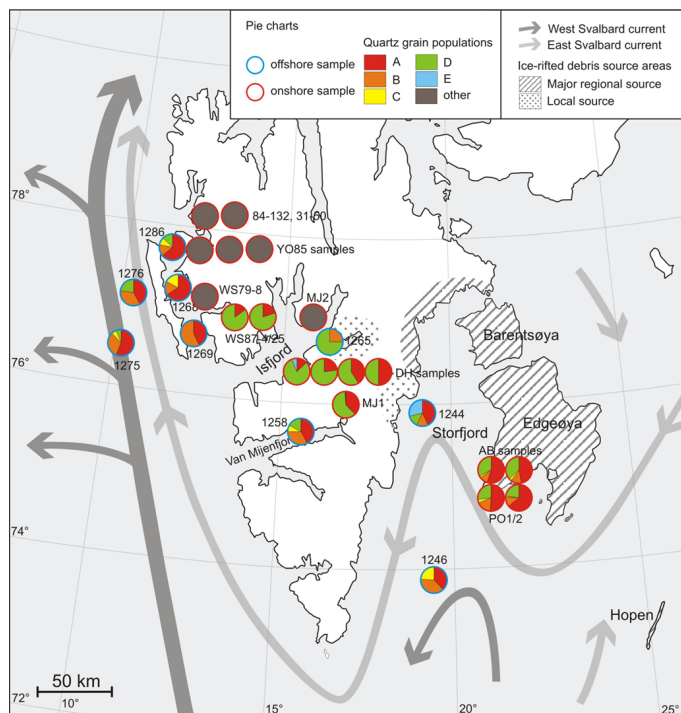


Fig. 5. Map of onshore and offshore samples of Spitsbergen and surrounding seas. Each pie chart represents the distribution of quartz grain populations (types A to E and “other”). The pie charts of offshore samples illustrate the dominance of type A and B grains in almost all samples whereas the onshore samples have distinct quartz populations restricted to certain areas. The distribution of quartz populations in the Late Triassic sandstones from Edgeøya resemble most the distribution in offshore samples even though the precision of the percentage of offshore grain populations is poor due to the limited number of accessible grains.

Title Page

Abstract

Introduction

Conclusions

References

Tables

Figures

⏪

⏩

◀

▶

Back

Close

Full Screen / Esc

Printer-friendly Version

Interactive Discussion

A new ice-rafted debris provenance proxy

A. Müller and J. Knies

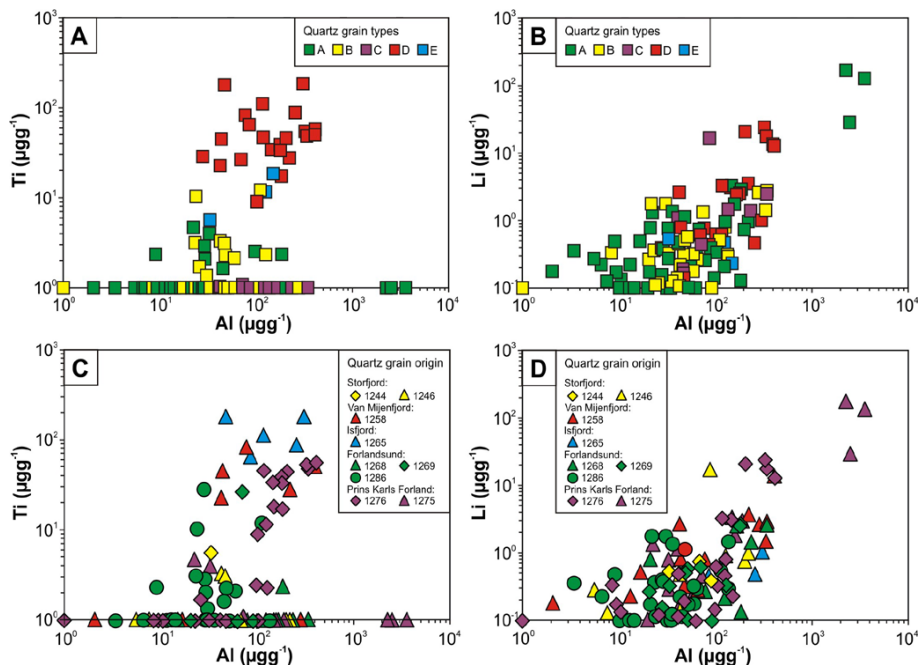


Fig. 6. Concentrations of Al versus Ti and Li of quartz grains in offshore samples. The same data are plotted, first, in respect to quartz type A, B and, second, to sample origin C, D. **(A, B)** – Type D grains have distinctive high Ti and relative high average Al and Li compared to the grain types A, B, C, and E. **(C, D)** – Samples 1265 (Isfjord), 1276 (Prins Karls Forland) and 1258 (Van Mijenfjord) have relative high proportions of grains with high Ti (D type grains).

[Title Page](#)
[Abstract](#)
[Introduction](#)
[Conclusions](#)
[References](#)
[Tables](#)
[Figures](#)
[◀](#)
[▶](#)
[◀](#)
[▶](#)
[Back](#)
[Close](#)
[Full Screen / Esc](#)
[Printer-friendly Version](#)
[Interactive Discussion](#)

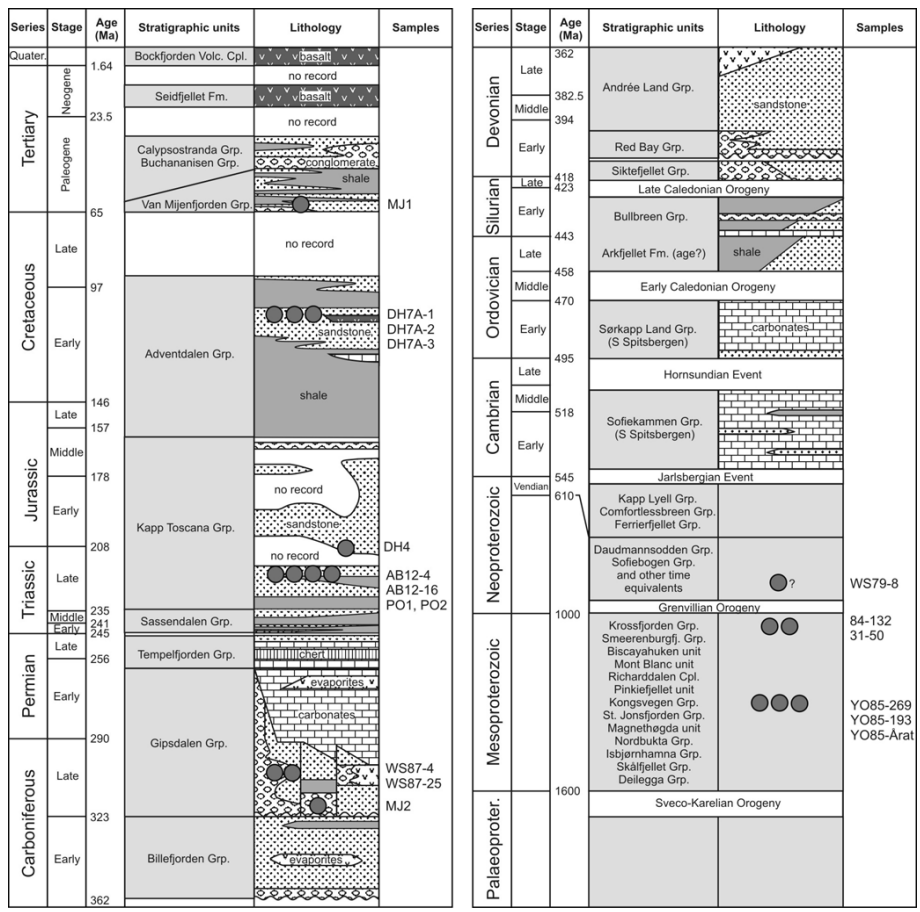



Fig. 7. Simplified geological timetable of Spitsbergen according to Dallmann (1999) and Dallmann et al. (2002) with stratigraphic positions of investigated onshore samples (dark circles).

A new ice-rafted debris provenance proxy

A. Müller and J. Knies

Title Page

Abstract

Introduction

Conclusions

References

Tables

Figures

◀ ▶

▶ ◀

◀ ▶

▶ ◀

Back

Close

Full Screen / Esc

Printer-friendly Version

Interactive Discussion



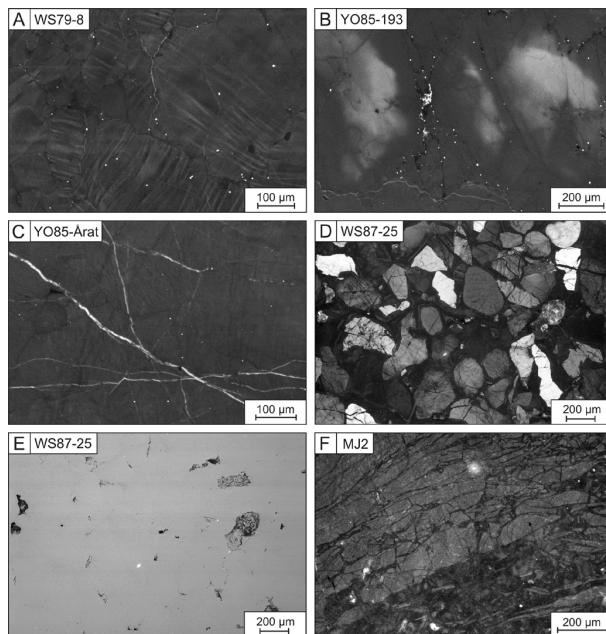


Fig. 8. SEM-CL and SEM images of quartz in onshore samples from Spitsbergen. **(A)** – Distinctive lamella-like CL structures in quartz of the Proterozoic metagranite from Vestkysten. **(B)** – Cloudy, bright luminescent domains in quartz with generally dull CL. Mesoproterozoic quartzite. **(C)** – SEM-CL image of quartz with moderate CL intensity crosscut by thin (< 5 μm), healed micro-fractures with bright CL. **(D)** – SEM-CL image of Permo-Carboniferous sandstone from the St. Jonsfjord. The majority of grains have bright CL and are overgrown by dull luminescent authigenic quartz. **(E)** – BSE image of the same sample domain as shown in D illustrating that the interstitial areas of dark CL represent authigenic quartz. **(F)** – SEM-CL image of chert from the Permo-Carboniferous Gipsdalen Group at Billefjord. Fragments of moderate bright luminescent chert are healed by a silica generation with dull CL.

A new ice-rafted debris provenance proxy

A. Müller and J. Knies

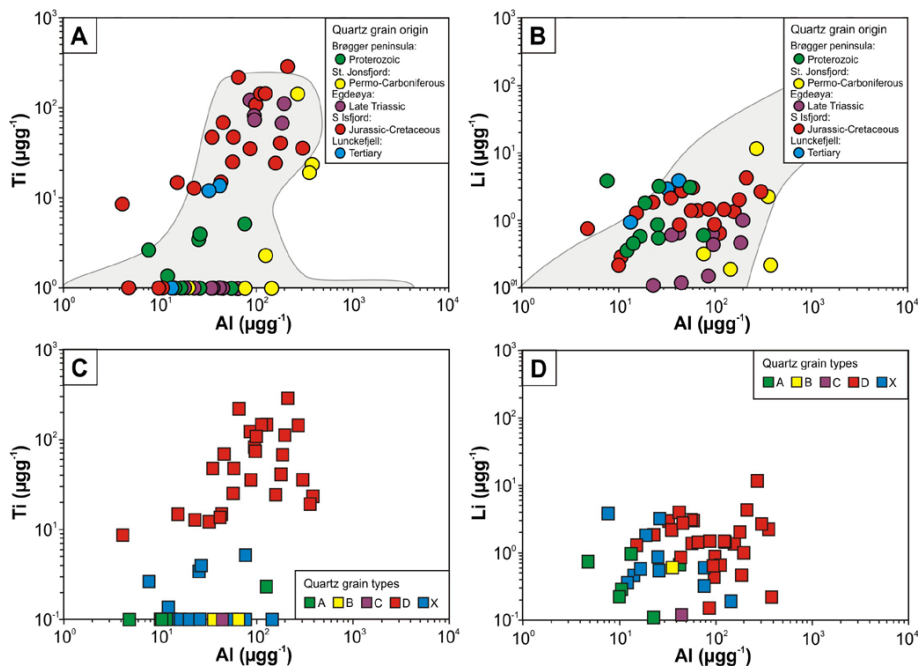


Fig. 9. Concentrations of Al versus Ti and Li of quartz grains in onshore samples. The same data are plotted, first, in respect to sample origin A, B and, second, to quartz type C, D. In general, the concentrations plot in the same range as the offshore samples (grey shaded areas). **(A, B)** – Samples from southern Isfjord are characterized by high Ti due to high proportion of D type grains (see **(C)**). **(C, D)** – Type D grains have distinctive high Ti and relative high average Al compared to the grain types A, B, C, and X. X type samples are quartz types which were not found in the offshore samples.

A new ice-rafted debris provenance proxy

A. Müller and J. Knies

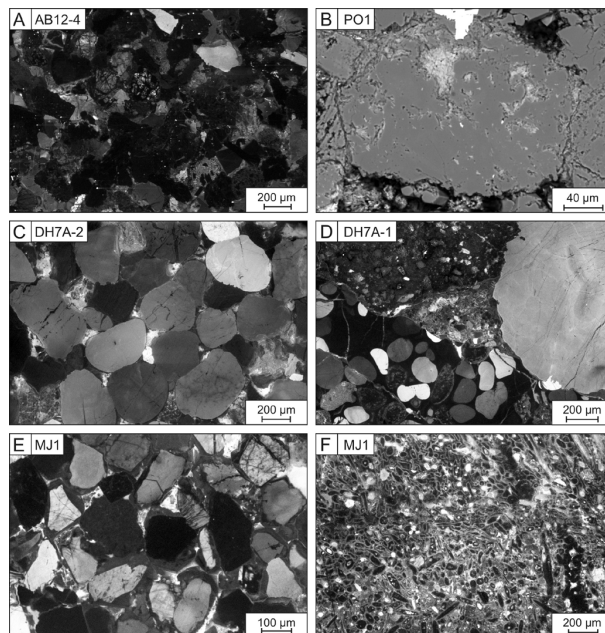


Fig. 10. SEM-CL and SEM images of quartz in onshore samples from Spitsbergen. **(A)** – SEM-CL image of Late Triassic sandstone from Edgeøya. The sub-angular quartz grains have predominantly weak CL, are partially overgrown authigenic quartz and cemented by sericite. **(B)** – BSE image of type B quartz grain of Late Triassic sandstone from Egdeøya with mica and feldspar micro inclusions. **(C)** – SEM-CL image of the Early Cretaceous sandstone from S Isfjord with predominantly bright luminescent quartz grains of type D. **(D)** – SEM-CL image of two fragments of fine-grained arkose and one bright luminescent type D quartz grain in Early Cretaceous sandstone from S Isfjord. **(E)** – SEM-CL image of the equi-granular, medium-grained matrix of the Tertiary conglomerate from Lunckefjell. The predominantly bright luminescent grains are overgrown by authigenic quartz with dull CL. **(F)** – SEM-CL image of a chert grain in sample MJ1 with distinctive structures.

Title Page

Abstract

Introduction

Conclusions

References

Tables

Figures

◀

▶

◀

▶

Back

Close

Full Screen / Esc

Printer-friendly Version

Interactive Discussion



A new ice-rafted debris provenance proxy

A. Müller and J. Knies

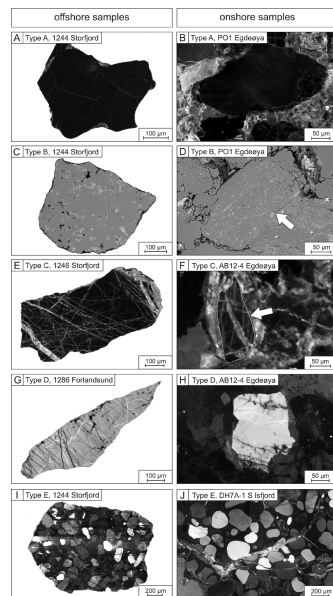


Fig. 11. SEM-CL and BSE images of quartz comparing grain types in offshore (left column) and onshore samples (right column). **(A)** – SEM-CL image of a dull luminescent, featureless type A grain with sericitic remains at the grain edge (brighter areas). **(B)** – SEM-CL image of a dull luminescent, featureless quartz grain of type A in Late Triassic sandstone from Egdeøya. **(C)** – BSE image of a type B quartz grain with common mica and feldspar inclusions. **(D)** – BSE image of a type B quartz grain (arrow) with common mica and feldspar inclusions in Late Triassic sandstone from the Egdeøya. **(E)** – SEM-CL image of a type C grain from offshore sample 1246. **(F)** – SEM-CL image showing a type C grain (arrow) in Late Triassic sandstone from the Egdeøya. **(G)** – SEM-CL image of a bright luminescent type D grain from offshore sample 1286. **(H)** – SEM-CL image of a bright luminescent type D grain in Late Triassic sandstone from the Egdeøya. **(I)** – SEM-CL image of an arkose fragment (type E) from offshore sample 1244. **(J)** – SEM-CL image of a large arkose fragment (type E) in Early Cretaceous sandstone from the southern Isfjord area.

[Title Page](#)
[Abstract](#)
[Introduction](#)
[Conclusions](#)
[References](#)
[Tables](#)
[Figures](#)
[Back](#)
[Close](#)
[Full Screen / Esc](#)
[Printer-friendly Version](#)
[Interactive Discussion](#)
